

Information in the Local Field Potential: Implications for Brain-Machine Interfaces

Gireeja Ranade



Electrical Engineering and Computer Sciences
University of California at Berkeley

Technical Report No. UCB/EECS-2009-121

<http://www.eecs.berkeley.edu/Pubs/TechRpts/2009/EECS-2009-121.html>

August 22, 2009

Copyright 2009, by the author(s).
All rights reserved.

Permission to make digital or hard copies of all or part of this work for personal or classroom use is granted without fee provided that copies are not made or distributed for profit or commercial advantage and that copies bear this notice and the full citation on the first page. To copy otherwise, to republish, to post on servers or to redistribute to lists, requires prior specific permission.

**Information in the Local Field Potential:
Implications for Brain-Machine Interfaces**

by

Gireeja Vishnu Ranade

S.B. Electrical Engineering and Computer Science,
Massachusetts Institute of Technology, 2007

A thesis submitted in partial satisfaction
of the requirements for the degree of

Master of Science

in

Engineering - Electrical Engineering and Computer Sciences

in the

GRADUATE DIVISION

of the

UNIVERSITY OF CALIFORNIA, BERKELEY

Committee in charge:

Professor Jose Carmena, Chair
Professor Michel Maharbiz

Spring 2009

Information in the Local Field Potential:
Implications for Brain-Machine Interfaces

Copyright © 2009

by

Gireeja Vishnu Ranade

Abstract

Information in the Local Field Potential:
Implications for Brain-Machine Interfaces

by

Gireeja Vishnu Ranade

Master of Science in Engineering - Electrical Engineering and Computer Sciences

University of California, Berkeley

Professor Jose Carmena, Chair

The last decade has seen a surge in the development of brain-machine interfaces (BMIs) as assistive neural devices for paralysis patients. BMIs are devices that decode neural activity to provide control signals for external devices, computers or prostheses. Current BMI research typically involves a subject playing a computer game or controlling a robotic prosthesis through neural activity (brain control). The local field potential (LFP) is a low frequency neural signal recorded from intra-cortical electrodes, and has been recognized as one containing movement information. This thesis investigates time and frequency properties of the LFP from the perspective of developing upper limb neuroprosthetic BMIs, and touches on three major topics.

First, the thesis considers LFP as a direct input for BMIs. The results in the thesis confirm previous studies that established the modulation of LFP spectral power by limb movement direction during manual control. However, in addition, it is observed that all signals from an electrode array show similar direction modulation. Basic offline movement prediction from only LFP information is also demonstrated. Second, the thesis explores coherence between two LFP signals. Results note that LFP signals across regions of the motor cortex are strongly coherent in the beta range (15 – 45 Hz) during stationary periods of manual control experiments. Some technical considerations for LFP-LFP coherence calculations are presented. Finally, brain control experiments with single unit action potentials controlling a computer cursor are considered. Findings in the thesis show that beta band LFP activity during brain control tasks closely resembles beta activity during tasks

involving direct limb movement. A last set of results indicate that the LFP beta band power can predict the movement state of a brain controlled cursor.

In conclusion, this thesis demonstrates the utility of the LFP as a supplementary information signal to develop the next generation of BMIs.

Contents

Acknowledgements	iii
1 Introduction	1
1.1 Brain-Machine Interfaces	1
1.2 Local Field Potential	3
2 Preliminaries	7
2.1 Surgery and Electrophysiology	7
2.2 Animal Behavior and Task	7
2.2.1 Linear Model	9
2.3 Data	9
2.4 Spectrum Estimation	10
3 Neural coherence	13
3.1 LFP-LFP Coherence: A technical discussion	14
3.1.1 Methods	18
3.2 Coherence Results	18
3.3 Discussion	20
4 Local field potentials as an input to brain machine interfaces	22
4.1 Direction Modulation	24
4.1.1 Modulation Methods	24
4.1.2 Modulation Results	25
4.2 Offline Movement Prediction	30
4.2.1 Prediction Methods	30
4.2.2 Prediction Results	30

4.3	Discussion	33
5	Beta band oscillations	35
5.1	Methods	36
5.1.1	Spike Triggered Averages	36
5.1.2	Prediction algorithm	37
5.2	Results	37
5.2.1	Spike triggered averages	40
5.3	Discussion	43
6	Conclusion	45
	Bibliography	48
	References	48

Acknowledgements

I thank my advisor, Jose Carmena, for his help with this project and general guidance regarding graduate school. Thanks to Professor Michel Maharbiz for comments on the final thesis draft.

The work in this thesis would not be possible without the experimental data collected by Karunesh Ganguly. I'm grateful to my lab-mates Rodolphe Heliot, Subramaniam Venkatraman, John Long and Amy Orsborn for valuable discussions. In particular, thank you very much Subbu for your detailed comments on the thesis and Neural Engineering paper, as well as your steady mentorship since I started grad school. Thank you Rodolphe for your technical and non-technical feedback and guidance, and for your help with the final submission.

I'm truly indebted to Ruth Gjerde, Shareena Samson and Rebecca Miller for their invaluable help in navigating the department. A special thanks goes to Krish Eswaran for his (gentle) encouragement to write, to Kris Woyach and Pulkit Grover for their friendship and support in Berkeley, and to all my friends, family and teachers from Pune, Cambridge, and Berkeley who made this thesis possible. And of course, thanks to my parents, Neelima and Vishnu Ranade, for their understanding and thus fending off "other issues" ☺, along with everything else.

This work was supported by a GAANN fellowship from the University of California, Berkeley (2007-2008) and a National Science Foundation Graduate Research Fellowship (2008-2009). Experimental work was funded in part by the Christopher and Dana Reeve Foundation.

Chapter 1

Introduction

About 200,000 patients in the United States suffer from total or partial body paralysis (e.g. paraplegics or quadriplegics) [1]. Spinal cord injuries nationwide lead to about 11,000 cases of permanent paralysis [1]. In 1980 Schmidt proposed that patients could employ direct interfaces to cortical centers to bypass an injured area (in the spinal cord, for instance) and thus perform voluntary actions [2]. Groundwork for these ideas was established in 1973, when Fetz and Baker demonstrated that given sensory feedback, a monkey could voluntarily adjust the firing rate of a specific cortical neuron to receive a reward [3].

1.1 Brain-Machine Interfaces

Brain-machine interfaces (BMIs) are devices that decode neural activity to provide control signals for external devices, computers or prostheses. A motor BMI system consists of a recording technology (e.g. intra-cortical or scalp electrodes), a decoder and decoding algorithm, a prosthetic limb and a visual feedback component. Neural signals are recorded from a subject, and are fed to a signal processing station (computer or chip). A decoding algorithm then computes a predicted movement trajectory for a robotic prosthetic arm, which then performs the movement. As with any control system, feedback is a key asset to a BMI system. Most current studies employ visual feedback to the subject for error correction and algorithm learning. In the future, intra-cortical micro-stimulation could be employed to provide this feedback. Finally, BMI studies have shown that neural plasticity

and volitional control of neural activity plays and will continue to play a tremendous role in the applicability of this technology [4]. Figure 1.1 shows a block diagram of this processing.

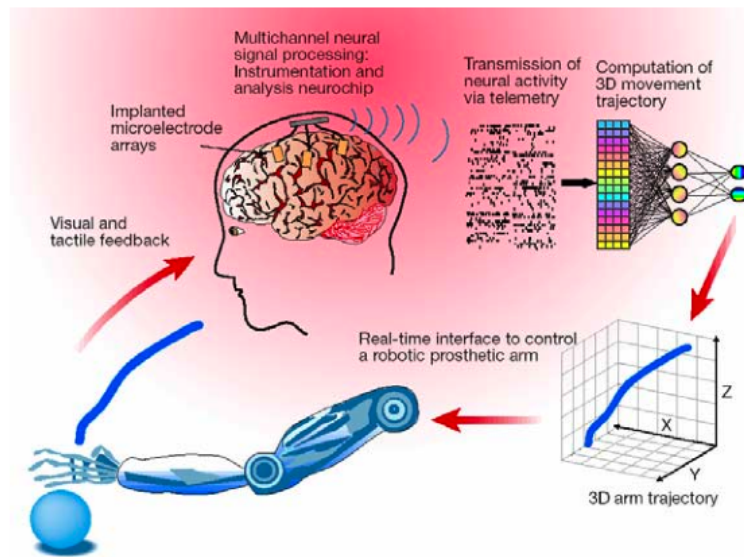


Figure 1.1. Schematic depiction of a BMI (Figure courtesy J. Carmena)

BMIs present not only an opportunity to drastically impact rehabilitation treatments but also a platform to further understand the adaptability and functionality of and communication mechanisms in the cortex. In 1999, Chapin et al. demonstrated rodent use of a BMI to control a robotic arm to obtain water [5]. Recent work to develop brain machine interfaces (BMIs) for neural prosthetics has tapped both noninvasive (electroencephalogram (EEG) and electrocorticogram (ECoG)) and invasive (local field potential (LFP) and single neuron action potentials) recordings as input to a movement decoder. More invasive technologies (micro-electrode arrays) offer cleaner recordings than less invasive ones (e.g. EEG) [6]. Single unit activity offers a high signal-to-noise ratio and can serve as an input control signal with multiple degrees of freedom [7]. A few groups have demonstrated the use of single unit activity to effectively control a computer cursor [8]–[10], as well as a robotic arm [10], [11]. Simple linear decoding models [10] as well as models based on the direction tuning of the single unit activity [11] have been used to predict motion of the cursor or robotic arm with visual feedback provided. Hochberg et al. has shown preliminary results for human BMI's and a tetraplegic was able to perform rudimentary actions with a robotic arm [12]. Other BMI systems solve classification or communication problems, by immedi-

ately identifying target position or choice (e.g. such as letters from a keyboard) eliminating the need to trace out a trajectory [13].

Numerous studies [14]–[16] have demonstrated the use of EEG signals in humans for applications ranging from the control computer cursors to rudimentary control of a wheelchair. The EEG signal on one electrode represents the activity of thousands of neurons recordings and can only resolve low frequencies of neural activity. The recordings suffer from a low signal-to-noise ratio and have very low spatial resolution [6]. ECoG signals are a more robust and noise-free alternative to EEG recordings, and have also been used for BMI applications [17], [18]. However, both EEG and ECoG may not be practical solutions for BMIs, since normal activities such as blinking or talking may cause high noise artifacts in both signals.

Despite the many promising results in the realm of intra-cortical invasive BMI, single unit recordings can be difficult to maintain for long periods of time. Micromotion of implanted micro-electrodes affects recording stability and insertion injury, chronic inflammation and glial encapsulation increases electrode impedance and limits the ability to record spikes over time [6]. LFP can be recorded from intra-cortical electrodes even under low impedance conditions, and could be used to supplement single unit decoders. Kennedy et al. used the LFP to control a computer cursor in one dimension and a virtual finger, with each LFP channel controlling one degree of freedom [19]. Mehring et al. [20] used a support vector machine to predict movement trajectories using LFP and showed that the discriminatory power of the signal for a 2-D task was similar to that of single-unit data.

This thesis explores the information content in LFPs, as a potential input to the next generation of BMIs.

1.2 Local Field Potential

Neural recordings from intracortical extracellular microelectrodes consist of two components superimposed on each other: action potentials from single and multi unit activity (spikes), and slow varying field potentials [21] (see figure 1.2). The high frequency spikes occur in between the 400-3000 Hz band of the signal, while the lower frequency recordings between 1-250 Hz are called the local field potential (LFP). The LFP relates well to sub-threshold integrative processes in dendrites and may reflect the synaptic activity in a ‘listening sphere’ around the tip of an implanted electrode [22]. It is also thought to

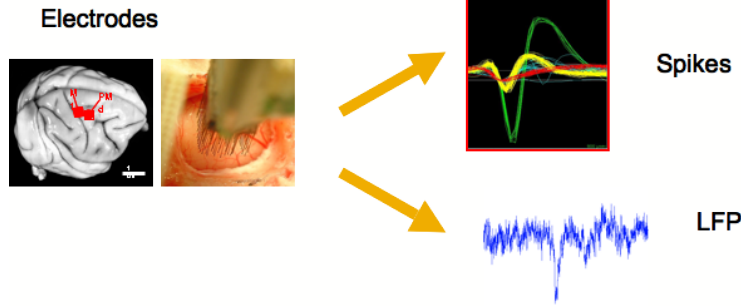


Figure 1.2. Neural recordings consist of spikes and local field potentials.

represent the summation of excitatory and inhibitory dendritic signals and other types of slow activity such as voltage dependent membrane oscillations or spike afterpotentials [21], [23]–[25].

The LFP signal is traditionally broadly divided into frequency bands. The division is not standard across the literature but mainly arises from characteristic oscillatory behaviors observed at the specific frequencies. Based on references and the data set, we defined the bands as shown in table 1.1

Table 1.1. LFP Bands

Band	Frequency Range	Thesis Definition
Theta	4-10 Hz [23], 4-8 Hz [26]	4-10 Hz [23]
Beta	10-30 Hz [23], 15-45 Hz [27], 20-40 Hz [28]	15-45 Hz [27]
Gamma	30-80 Hz [23], 40-70 Hz [29], 25-90 Hz [30]	60-100 Hz

It is observed that the power frequency (f) of the LFP (and EEG) is inversely proportional to f . Thus widespread slow events may modulate faster local events and small changes at the lower frequencies can lead to a cascade of energy dissipation in higher bands [23].

Our knowledge about the information content in LFPs is limited compared to the current understanding of neural spiking patterns. Recent work has shown many correlations between oscillations in the LFP bands and behavior, and new properties of the signal have been discovered. Some interesting results that help us understand the LFP follow, and this thesis builds on them from the BMI perspective.

1. **The origin of LFP:** The origin and functionality of the LFP signal are largely debated in the community. One theory suggests that the LFP mostly represents

the inputs to a particular brain region and local processing taking place around the recording electrode, while the spikes represent the outputs generated by the region. Thus, the LFP and spikes recorded on the same electrode may represent information from distinct sources [25]. Alternatively, Belitski et al. examined correlations between the stimulus and, spikes and LFP recorded on the same electrode in the visual cortex of an anesthetized macaque while presenting a color movie [21]. They found signal and noise correlations between the high gamma band and spikes, however, LFP < 40 Hz showed little correlation with high frequency bands or with spikes, suggesting that the processes generating the two signals are decoupled. This contrasts with Nicolelis et al. who report correlations between spikes and the 8 – 10 Hz LFP signal [31].

2. **Gamma coherence relates to behavior and information transfer:** Spike-field coherence and oscillatory synchrony may subserve neuronal communication (for a review, see [32]), and have been related to attentional states. Gamma band spike-field coherence in the visual cortex has been shown to increase with attention to a stimulus [33]. The degree of gamma synchronization prior to and during a behavioral change was correlated with response times to that change [29]. Gamma frequency oscillations may also predict spike response latency [34].
3. **Propagating beta oscillations:** During a motor task, oscillations in the beta range propagate spatially across the motor cortex along dominant spatial axes [27], and may assist inter- and intra- cortical information transfer.
4. **LFP in parietal cortex:** LFP in the posterior parietal cortex has a temporal structure that varies with behavior and can predict behavioral state (e.g. planning a reach or a saccade) and the direction of the currently planned movement from single trial information [22]. Power in the gamma band in the lateral intraparietal area increased during a memory recall task, as did spike-LFP coherence [30].
5. **Applications to BMI and direction tuning:** As mentioned in section 1.1 the LFP signal has potential for BMI applications. In addition, power in frequency bands of the LFP and evoked potentials are modulated with movement direction [7], [35].
6. **Beta oscillations are related to movement state:** Changes in LFP oscillations are constant with behavioral changes. In the motor cortex, LFP oscillations in the beta range increase with posture hold and decrease with movement during a motor task [27], [36], [37]. Murthy and Fetz observed strong beta oscillations during unconstrained exploration, when compared to rest periods [28].

7. Computational models of information transfer in the brain: Computational models suggest oscillation based synchrony may be the most energy efficient physical mechanism for temporal coordination in the brain [23]. Oscillations periodically elevate the membrane potential, providing a preferential response period for neural response [38]. Other models and data suggest that network oscillations may be useful for (1) the representation of information (2) the regulation of information flow and (3) information storage and retrieval [39].

These studies demonstrate the potential for LFPs as inputs to BMIs, and suggest low frequency oscillations may play a critical role in inter- and intra- cortical communication and synchronization. This thesis examines the information content and properties of LFP signals in the contralateral and ipsilateral motor cortex, towards harnessing them as BMI control signals and exploring the role of characteristic intra-cortical oscillations. To this end, detailed data analysis techniques for spectrum and coherence estimation in neural signals are discussed. The thesis is addressed to both neuroscientists who wish to explore the properties of LFPs and spectral estimation techniques, as well as engineers who may want an introduction to the science of BMIs and LFPs.

Chapter 2

Preliminaries

This chapter describes the behavioral experiment, data collection and preliminary data analysis. All results in this thesis used offline data. The author was not involved in the data collection. All experimental data was collected by members the Carmena Lab.

2.1 Surgery and Electrophysiology

All procedures conducted for this research complied with the National Institute of Health *Guide for the Care and Use of Laboratory Animals*. They were approved by the Institutional Animal Care and Use Committee at the University of California, Berkeley. Two adult male rhesus monkeys (*Macaca mulatta*) were chronically implanted in the primary motor cortex (M1) with bilateral arrays of 64 teflon-coated tungsten microelectrodes (35 micrometers in diameter, 500 micrometers separation between microwires) in an 8x8 array configuration (CD Neural Engineering, Durham, NC). A 128-multichannel acquisition processor (Plexon Inc., Dallas, Texas, United States) simultaneously recorded single neuron and multiunit activity.

2.2 Animal Behavior and Task

The subjects were trained to perform a center-out task to eight targets while seated in a KINARM exoskeleton (BKIN Technologies, Ontario, Canada). This center-out task

involved reaching to one of eight peripheral targets from a center hold point, and was presented as a video game on a horizontal computer screen.

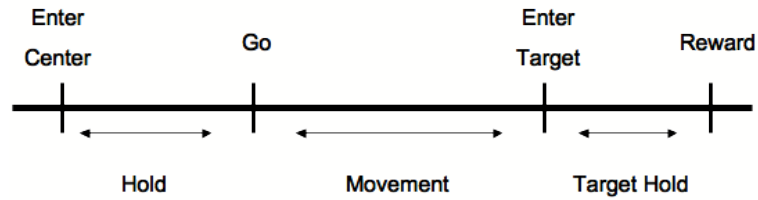


Figure 2.1. Structure of center-out task with variable hold period. (Figure courtesy K. Ganguly)

Figure 2.1 shows the task structure, and figure 2.2 is a cartoon of the subject performing the task. To initiate a trial, the subject would bring the cursor to the center target, which led to the appearance of the peripheral targets. Following a random hold period (HP) between 500 – 1500 ms, the go cue was presented by the center target changing color. Failure to hold the cursor in the center for the hold period caused an error. After the go cue, the subject reached for the indicated target (called the movement period (MP)) and held the cursor at that position for 500 ms (called target hold period (THP)) to receive a juice reward. The non-task arm was held in place during the task by a splint.

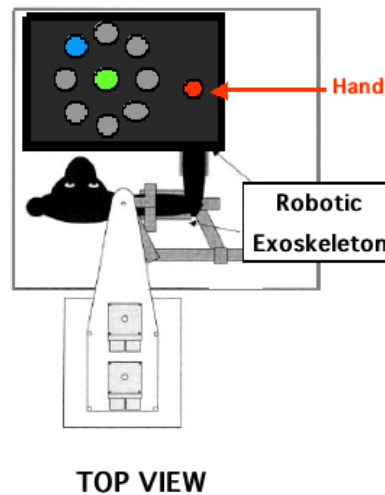


Figure 2.2. Center-out task: Seated in a KINARM, the subject must reach from the center target to indicated peripheral target upon presentation of the go cue.

Subjects performed the task under two settings: manual control (MC) mode and brain control (BC) mode. Under MC subjects could move their hand directly underneath the screen to move an on-screen cursor co-located with the hand. Under BC, a linear filter

(see below) was used to predict cursor position based on neural ensemble activity. Hand movements in this case could not directly affect cursor position.

Under manual control the subject could move his hand directly underneath the screen to move an on-screen cursor that represented his hand and was located directly above it. A linear filter (see below) was used to predict cursor position based on neural ensemble activity under brain control mode. Hand movements in this case could not directly affect cursor position and the subject's hand remained stationary.

2.2.1 Linear Model

As in previous work [10], a Wiener filter was used to predict cursor position from the activity of an ensemble in M1 during BC. Neural firing rates over 100 ms bins were used as input to the model. The model parameters were trained and fixed using ten minutes of data. Position was predicted based on the neural activity at that time and the history of activity for the past second.

2.3 Data

Each recording session lasted about 2 – 3 hours per day, during which the subject performed $\sim 100 - 200$ trials in MC and BC modes. The subject was over-trained in the MC task; a reach took ~ 1 s. Reaches in the BC mode often did not follow the straight line path to the target, had a stop-go structure as the animal attempted to reach the target and took much longer ($\sim 3 - 10$ s). Observations of the subject during task performance noted no overt arm movements in BC mode.

LFPs between 0 – 150 Hz were recorded at a sampling frequency of 1 KHz on each electrode. All algorithms for data analysis were implemented in MATLAB. Cursor position in MC and BC was recorded in joint coordinates, which consists of the angles made by the shoulder and elbow joint. Jacobian conversion was used to derive cartesian co-ordinates from the shoulder and elbow angles.

The KINARM measured and recorded cursor position during both manual and brain control modes. Instantaneous velocity of the cursor was calculated as the position differences over a 20 ms window and smoothed with a 10 Hz lowpass filter.

2.4 Spectrum Estimation

Minimizing the noise in spectral estimates of the LFP signal is an essential prerequisite to establish correlations between oscillations in specific frequency bands and behavior. Such estimates are generally subject to two sources of errors - the first being noise inherent in the recording and the second being errors introduced by the particular parameters of the estimation technique (e.g. window size and finite signal length). A general analysis of different spectral estimation techniques is found in [40], and specific commentary on these techniques for neural data analysis is found in [41]. We chose the multitaper technique for this thesis as a method to maximally de-correlate the finite-window size correlations introduced in neighboring frequencies [41]. The technique averages independent estimates of the spectrum, thereby reducing the recording noise. We compute the spectral estimates of short data windows to construct spectrograms as detailed below.

Specifically, the problem set up is as follows: consider a signal $x(t)$ of finite length N . Let $(-W, W)$, $0 < W < \frac{1}{2}$, be the frequency resolution we want to achieve. Window-size in the time domain and frequency resolution are the fundamental tradeoff parameters in spectral estimation. Sharp concentration in frequency (a delta function) requires an infinite sequence length in the time domain. Finite time sequences are thus inherently limited in their spectral concentration. The *discrete prolate spheroidal sequences* (DPSS), $U_k(N, W; f)$ with $k = \{0, 1, 2 \dots K-1\}$, for the bandwidth-time product NW are orthogonal windowing functions (and thus of finite length) that have the greatest energy concentration in $(-W, W)$ [42]. Spectral concentration of a frequency domain function H in the window $(-W, W)$ is defined as

$$\lambda = \frac{\int_{-W}^W |H(f)|^2 df}{\int_{-\infty}^{\infty} |H(f)|^2 df} \quad (2.1)$$

For fixed NW , at most $2 \cdot NW$ windows can have a concentration (λ) close to 1, which limits $k < 2 \cdot NW$, and thus the amount of smoothing we can achieve [42]. Each windowing sequence $U_k(N, W; f)$ is called a taper. Details of this can be found in [42] and [43], which also plots some sample plots of sequences. We use the DPSS as an orthogonal basis to decompose $x(t)$ and calculate independent spectral estimates. The spectrum is calculated using K tapers as

$$X_k(\omega) = \sum_{t=0}^{N-1} x(t) U_k(N, W; f) e^{-j\omega t} \quad (2.2)$$

$$X(\omega) = \frac{1}{K} \sum_{k=0}^{K-1} X_k(\omega), \quad (2.3)$$

and the power spectral density (PSD) is

$$S_{xx}(\omega) = X(\omega) \cdot X^*(\omega). \quad (2.4)$$

This technique for spectral estimation is also known as the *Slepian taper* or *multi-taper* method. We used the MATLAB functions `dpss` and `pmtm` to implement the algorithm, with time-bandwidth product $NW = \frac{5}{2}$ and $K = 2 \cdot NW = 5$ tapers. The maximum value of NW generally used is 4, however, increasing NW increases computation time and we did not find significant improvements by going beyond $NW = \frac{5}{2}$. (Note: The Chronux toolbox also provides functions to implement multi-taper spectral analysis [44], [45]). Following this, spectrograms were calculated every 50 ms using a sliding window of 200 ms, thus the spectral decomposition at time t was calculated using the signal between $[t - 100, t + 100]$ ms. Average spectrograms were computed aligned to the go cue and the movement onset. Figures in this thesis are referenced to the movement onset and presented on a logarithmic scale with arbitrary but uniform power units across figures. However, we observed similar results with respect to go cue.

In order to remove the effects of any common noise that may be recorded on the ground reference electrode, we examined two conditions: (1) spectrograms of the recorded raw LFP signals and (2) spectrograms of each LFP signal re-referenced to the average over all LFP signals. However, this re-referencing does not make a significant qualitative difference to the spectral estimates, and spectrograms in this thesis do not use re-referenced signals.

Figure 2.3 shows a representative spectrogram of a single trial, as well as the average spectrogram over all trials in the session. The gamma band contains the least power, as expected from the $\frac{1}{f}$ power characteristic of the LFP. Power in the beta band decreases with movement onset consistent with results from [36], [37]. This phenomenon is further explored in chapter 5. Power in the theta band shows some oscillatory behavior, but we did not investigate this further.

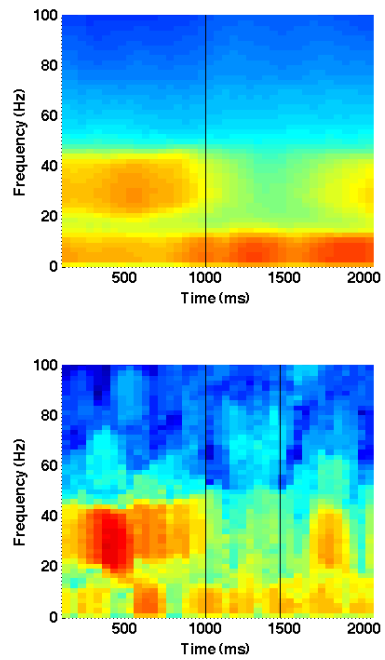


Figure 2.3. Representative spectrograms delineated by task structure. Go cue was presented at 1000 ms. Top: Average spectrogram over ~ 900 trials. Bottom: Single trial spectrogram. Subject enters target on second black line.

Chapter 3

Neural coherence

Oscillatory behavior in neural recordings has been widely observed across recording technologies and frequency bands since Berger in 1929 described the 8 – 12 Hz alpha oscillation in electroencephalogram (EEG) recordings [46]. Some functional interpretations of these oscillatory behaviors include higher order sensory processing, inter- and intra-cortical communication, facilitation of synaptic plasticity and long-term information consolidation; however, given the difficulty in connecting the oscillations with behavior, these interpretations are debated [23], [39], [47]. In-vitro experiments establish the physiological impact of oscillations. For instance, a sinusoidal current imposed on an axon affects both its output and its sensitivity to input spikes [38], [48].

Signal coherence has been used with EEG signals as an effective tool for the study of synchronous oscillatory behavior [49]. Coherence can be thought of as a measure of the linear coupling between two signals. Recent work has focused on spike-LFP coherence as a measure of the phase coupling between spike timing and LFP oscillation [29], [50], [51]. Coherence between field potential oscillations and electromyogram (EMG) activity has been investigated as a mechanism for communication [52]. However no results thus far have investigated coherence between LFP signals.

Spike-field coherence and oscillatory synchrony may subserve neuronal communication (for a review, see [32]) and may also be related to attentional state. In a visual change-detection task, gamma band spike-field coherence in the visual cortex was higher for an attended stimulus than an unattended one [33]. The degree of gamma synchronization in the cortex prior to and during a behavioral change was correlated with response time to

that change [29]. Gamma frequency oscillations may predict spike response latency [34]. Gamma band coherence between the motor cortex and the spinal cord neurons during a change-detection task is correlated with modulations in a subject’s readiness to respond [52]. Characteristic coherent beta rhythms are observed in field potential activity during posture hold and exploratory activity. These beta rhythms can be synchronized with limb EMG activity [28], [37], [53].

Low frequency delta band (0.5-4 Hz) oscillations in the visual cortex entrain to visual stimuli presented in a rhythmic stream. The high excitability phases tend to coincide with events of the attended stream. The phase of the delta oscillation also determines momentary power in higher frequencies [54]. Similarly, the phase of the theta band can be coupled with the power in the high gamma band and the coupling between the two bands changes with subject behavior [26]. These results both suggest a functional importance for oscillations in effective communication during cortical processing.

Murthy and Fetz observed that units in the ipsilateral and contralateral cortices synchronize during oscillatory periods [55]. Movement related desynchronization has been observed in both hemispheres even though only one limb was moved [49].

In this chapter we set the groundwork to explore cortical LFP coherence as means of communication in the brain. The first section deals with technical considerations for coherence calculations, while the latter gives examples of cortical coherograms and explores changes in coherence with behavior.

3.1 LFP-LFP Coherence: A technical discussion

The coherence (C_{xy}) between two signals $x(t)$ and $y(t)$ is defined as the product of their cross spectral density (S_{xy}) normalized by square root of the product of their power spectral densities (S_{xx}, S_{yy}) as in equation 3.1

$$C_{xy}(\omega) = \frac{S_{xy}(\omega)}{\sqrt{S_{xx}(\omega) \cdot S_{yy}(\omega)}} \quad (3.1)$$

We assume that $x(t)$ and $y(t)$ are stationary for the remainder of this discussion. C_{xy} is a complex quantity such that $0 < |C_{xy}|^2 < 1$ [56]. $C_{xy}(\omega) = 0$ for every ω if x and y are linearly independent. If the signals are linearly related, i.e. $y(t) = h(t) * x(t)$, such that $H(\omega) = A(\omega) \cdot e^{-j\theta(\omega)}$, then $C_{xy}(\omega) = e^{j\theta(\omega)}$. As shown in [56], the coherence can also be

interpreted as a measure of the relative linearity of the two signals. Thus, if $H_o(\omega)$ is the optimal linear predictor for $y(t)$ based on $x(t)$, then $C_{xy}(\omega) = H_o(\omega) \sqrt{\frac{S_{xx}(\omega)}{S_{yy}(\omega)}}$.

The correlation coefficient of two zero mean random variables X and Y is given by

$$\rho_{XY} = \frac{E[XY]}{\sqrt{E[X^2] \cdot E[Y^2]}}, \quad (3.2)$$

where $E[\cdot]$ is the expectation operator. Observing the similarity of equations 3.1 and 3.2, we see that C_{xy} can be interpreted as the correlation coefficient of the Fourier components of $x(t)$ and $y(t)$ at ω . Thus, it is meaningless to calculate the coherence between two finite length signals over only one window. To circumvent this issue we may divide each signal into smaller segments and calculate coherence over these pairs of segments. Alternatively, repeated trials of the experiment under identical conditions can provide a set of finite length signals over which we may calculate the coherence (note that the stationarity of signals across trials is an important assumption).

It is important to consider the effect of finite window size when calculating coherence, as illustrated in the following calculation. Let $x[n]$ and $y[n]$ (sampled versions of $x(t)$ and $y(t)$) be finite length discrete time signals of length N , with support on 0 to $N - 1$. Then the Fourier transforms of $X(\omega)$ and $Y(\omega)$, the cross-correlation $r_{xy}[n]$ and S_{xy} are given as (see [40])

$$X(\omega) = \sum_{n=-\infty}^{\infty} x[n]e^{-j\omega n} = \sum_{n=0}^{N-1} x[n]e^{-j\omega n} \quad (3.3)$$

$$Y(\omega) = \sum_{n=-\infty}^{\infty} y[n]e^{-j\omega n} = \sum_{n=0}^{N-1} y[n]e^{-j\omega n} \quad (3.4)$$

$$r_{xy}[n] = E_m [x[n+m] \cdot y[m]], \quad m \text{ uniform over } 0 \text{ to } 2N-1 \quad (3.5)$$

$$S_{xy}(\omega) = \sum_{n=-\infty}^{\infty} r_{xy}[n]e^{-j\omega n} = \sum_{n=0}^{2N-1} r_{xy}[n]e^{-j\omega n} \quad (3.6)$$

where $E_m[\cdot]$ is the expectation operator over m . Note that the definition of r_{xy} in equation 3.5 uses the fact that both $x[n]$ and $y[n]$ have finite support. Using equation 3.5 and 3.6,

$$S_{xy}(\omega) = \sum_{n=-\infty}^{\infty} E_m [x[n+m] \cdot y^*[m]] e^{-j\omega n} \quad (3.7)$$

$$= \sum_{n=-\infty}^{\infty} E_m [x[n+m] \cdot y^*[m]e^{-j\omega n}] \quad (3.8)$$

$$= \sum_{n=-\infty}^{\infty} E_m \left[x[n+m]e^{-j\omega(n+m)} \cdot y^*[m]e^{j\omega m} \right] \quad (3.9)$$

$$= E_m \left[\sum_{n=-\infty}^{\infty} \{x[n+m]e^{-j\omega(n+m)}\} y^*[m]e^{j\omega m} \right] \quad (3.10)$$

$$= E_m \left[X(\omega) \cdot y^*[m]e^{j\omega m} \right] \quad (3.11)$$

$$= X(\omega) \cdot E_m \left[y^*[m]e^{j\omega m} \right] \quad (3.12)$$

$$= X(\omega) \cdot \frac{1}{2N} \sum_{n=0}^N y^*[m]e^{j\omega m} \quad (3.13)$$

$$= X(\omega) \cdot \frac{1}{2N} \sum_{n=-\infty}^{\infty} y^*[m]e^{j\omega m} \quad (3.14)$$

$$= X(\omega) \cdot \frac{1}{2N} \cdot Y^*(\omega) \quad (3.15)$$

3.10 goes through because of the linearity of expectation, 3.11 uses the definition of the Fourier transform. To get 3.13 we use the fact that $y[n]$ has finite support, and use this again to get 3.14. Thus the window size N affects S_{xy} at every frequency ω .

Now,

$$X(\omega)Y^*(\omega) = \sqrt{S_{xx}(\omega) \cdot S_{yy}(\omega)} \cdot e^{-\theta(\omega)}, \quad (3.16)$$

where $\phi(\omega)$ is the phase of $X(\omega)Y^*(\omega)$, which gives

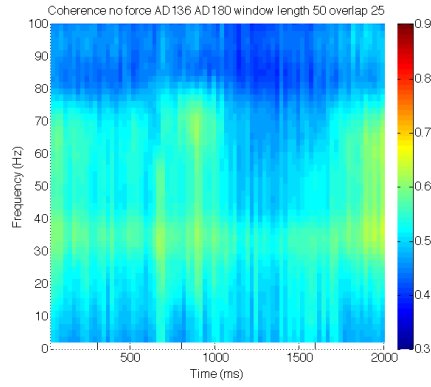
$$C_{xy} = \frac{\frac{1}{2N} X(\omega)Y^*(\omega)}{\sqrt{S_{xx}(\omega) \cdot S_{yy}(\omega)}} \quad (3.17)$$

$$= \frac{1}{2N} \cdot e^{\theta(\omega)}. \quad (3.18)$$

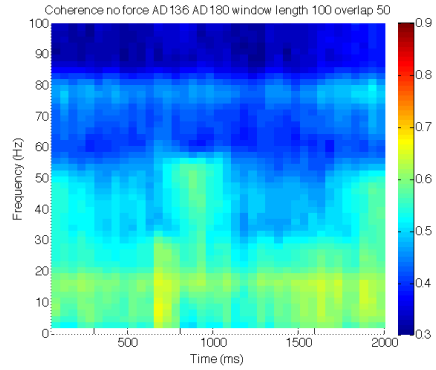
Thus even for signals that may be linear transformations of each other, as noted above the coherence will be affected by the $\frac{1}{2N}$ factor related to the finite window size.

Figures 3.1(a) - 3.1(f) investigate the coherence between the signal on two electrodes AD180 and AD136 with window sizes varying from 50 ms to 1000 ms. The effect of the window scaling factor of $\frac{1}{2N}$ is apparent. At the same time, within each figure, certain prominent features still stand out, such as the increase in coherence around 1000 ms. This analysis and the figures suggest that performing analysis with different window sizes for different frequencies may introduce artifacts in the coherence values obtained. Coherence calculations using different windows should be normalized before they can be compared.

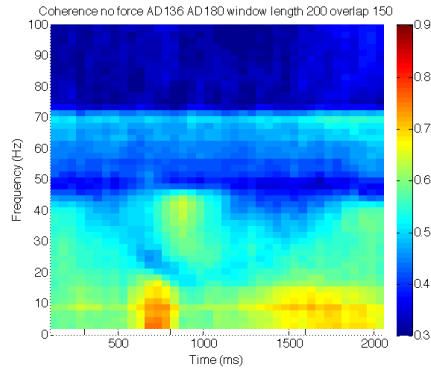
Care must be taken in re-referencing signals to a common average signal for coherence



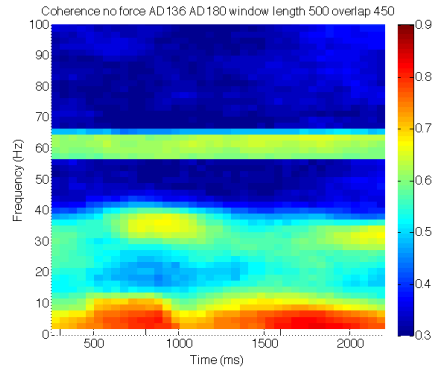
(a) 50 ms window with 25 ms overlap



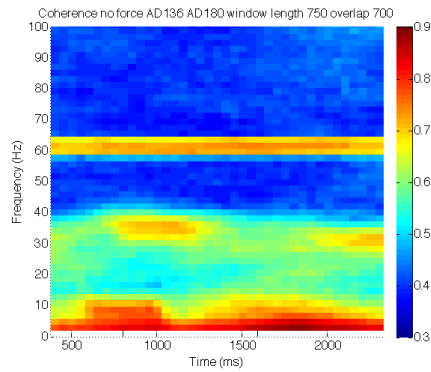
(b) 100 ms window with 50 ms overlap



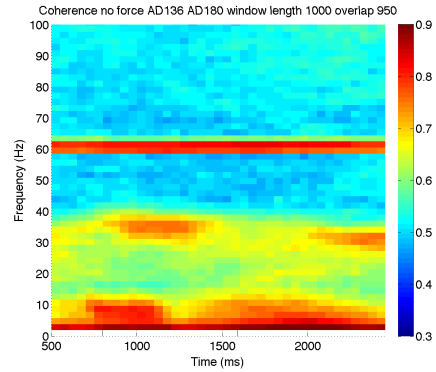
(c) 200 ms window with 150 ms overlap



(d) 500 ms window with 450 ms overlap



(e) 750 ms window with 700 ms overlap



(f) 1000 ms window with 950 ms overlap

Figure 3.1. Coherence between electrodes AD180 and AD136 using different window sizes

calculations. Common noise in both signals could directly affect the coherence between them, and thus it is important to remove this signal. However re-referencing a signal to the common average in the absence of a common noise signal could introduce an artifactual coherence due to the added components from the average. There is no obvious method to determine if there is noise on a reference electrode, and thus we compared coherence estimates with and without re-referencing. All coherograms in this chapter use re-referenced signals.

3.1.1 Methods

The multitaper method can be used to estimate the cross spectral density, S_{xy} , exactly as the power spectral density, S_{xx} , was estimated in section 2.4, using the relationship

$$S_{xy}(\omega) = X(\omega) \cdot Y^*(\omega) \quad (3.19)$$

in place of equation 2.4; further details can be found in [43]. This was implemented based on software developed by Huybers [57] using the `dpss` function from MATLAB. As noted in [41], [43] the coherence estimate is subject to a bias offset, which was also considered in the estimation. Time-bandwidth product, number of tapers for coherence calculation and the sliding window parameters remain as used in section 2.4. Other considerations for coherence estimation are given in section 3.1. We fixed the window size as 200 ms for all analysis other than the comparison of window sizes shown in figure 3.1.

3.2 Coherence Results

From figure 3.1 we can see that coherence is maximal in the beta range just prior to movement onset during the hold period, but no significant coherence in the gamma or theta ranges is seen. (Strong coherence around 60 Hz for larger window sizes is due to electrical noise.)

Coherence between two electrodes from M1 varied with the separation between them. Figures 3.2 and 3.3 plot coherograms across the entire M1 array with respect to a single electrode as noted. Coherence is very high in all frequency ranges for proximal electrodes. As the distance between electrodes increases, coherence is observed only during strong beta oscillations.

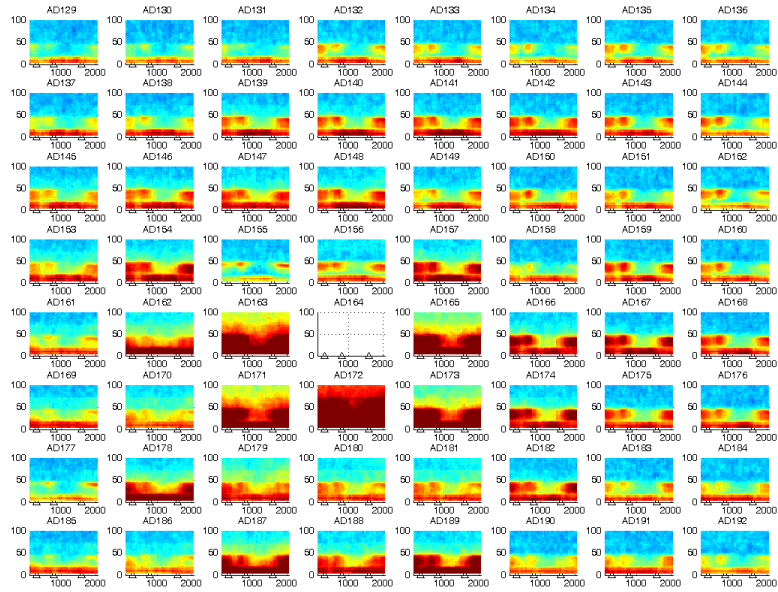


Figure 3.2. Coherence across the entire implanted M1 array, with respect to AD164 (blank rectangle).

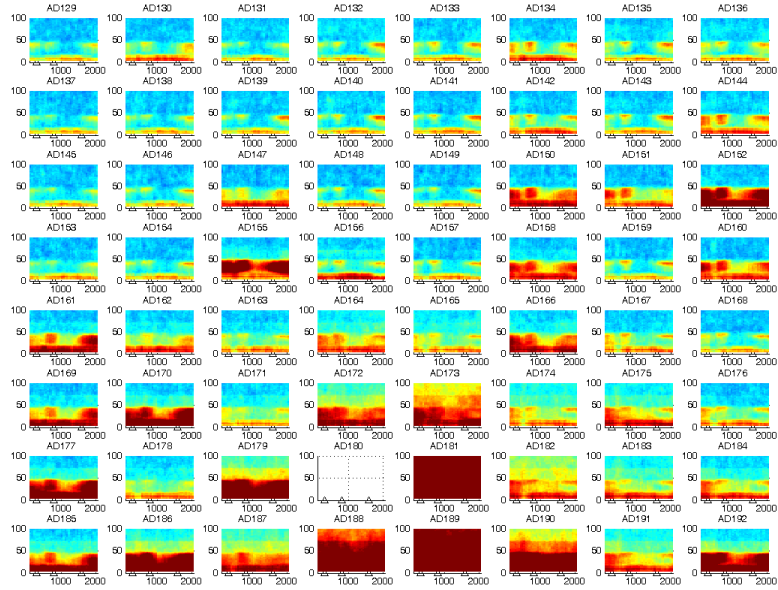


Figure 3.3. Coherence across the entire implanted M1 array, with respect to AD180 (blank rectangle).

We found that LFP recordings from the motor cortex of the right hemisphere (ipsilateral M1) are similar to recordings from the left hemisphere (contralateral M1) during tasks performed with the right hand, which is consistent with the results of [55]. Indeed, the trial-spectrogram of the ipsilateral cortex is qualitatively the same as that for the contralateral (figure not shown). A wiener filter allowed predictions of the ipsilateral LFP during beta oscillations from the contralateral with correlations as high as 0.7. Prediction accuracy was lower during the execution period.

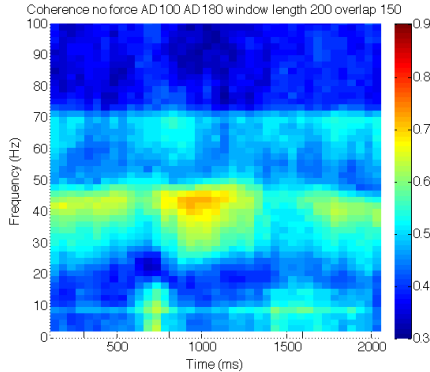


Figure 3.4. Coherence between M1 and M1 ipsilateral, with a 200 ms window.

Figure 3.4 shows the coherence between signals from the contralateral and ipsilateral cortices. Once again, the coherence pattern resembles the coherence between two of the further contralateral electrodes. The coherence between the two hemispheres is maximum in the beta band during oscillatory activity, reinforcing the widespread nature of these oscillations.

3.3 Discussion

Our analysis shows the highest coherence in the beta range just prior to movement onset. The drop in coherence coincides with the drop in beta power in the LFP signal. Technically, the amplitude of two signals should not affect the coherence between them, since our calculations involve normalizing by the PSDs of each signal. However, a finite window size may introduce some artifacts in the calculation. We did not quantify the relationship between the drop in beta power and the drop in coherence, and these may or may not be related.

Compared to the beta range, there is very little coherence observed in the gamma range.

It is well known that spikes phase lock to beta oscillations during a task hold period [28], [37]. We observe beta coherence during the hold period in M1 as well as across hemispheres. Could this coherence serve as a mechanism for spike synchronization? Spikes may phase lock to local oscillations in either hemisphere allowing them to synchronize with each other. The beta oscillations act as a clocking mechanism for the spikes. However, the causality between the spike-synchronization and coherence is unclear. Alternatively, it is possible that synchronized spiking may be the cause for widespread beta coherence.

We observed widespread synchronous beta oscillations during the hold period. These oscillations extended to both the ipsilateral cortex and the PMd (results for PMd not shown). Is this oscillation used to synchronize spike timing across brain regions? It is well known that spikes phase lock to beta oscillations [28], [37]. It is interesting to note that even LFPs on very distant electrodes show beta coherence during the hold period, when no other frequencies are coherent at such long distances. Alternatively, is the beta just an idle oscillation of the brain - a default low energy resting state?

This chapter develops some techniques to calculate LFP-LFP coherence. However, the significance of this measurement or potential implications for understanding LFP functionality are yet to be fully investigated.

Chapter 4

Local field potentials as an input to brain machine interfaces

As described in the introduction to this thesis, time and frequency analyses of the LFP attest to the abundance of information contained in this signal. Given the difficulties associated with single-unit recordings of spike data [6], it is natural attempt to directly utilize the LFP for BMI applications. In this light, this section explores the use of LFP for BMI.

Previous work by Kennedy used LFPs for one-dimensional control of a computer cursor and virtual finger [19]. Mehring and colleagues were able to use a support vector machine to predict movement trajectories from LFP recordings with the average correlation coefficient around 0.7 [20]. In addition to direct trajectory prediction, it is important to harvest all possible information from the signal. Given the directional tuning observed in spike data [58], an obvious question is: is the LFP modulated by direction?

Georgopoulos et al. [58] found that limb movement direction can be predicted by the activity of a population of motor neurons. They found that some neurons modulate their firing rate in accordance with the direction of movement; the direction that elicits maximal firing rate relative to a baseline is called the *preferred direction* of the neuron. The neuron is said to be *tuned* to that direction. Georgopoulos found that different neurons are tuned to different directions and thus the instantaneous firing rates of a neural ensemble could be used to decode the direction of the current movement. The direction indicated by the

ensemble is called the *population vector* and is calculated as the vector sum of the preferred directions of each cell, weighted by the instantaneous firing rate.

Rickert et al. [35] reported that movement direction (for a 2D center out task) is encoded in the LFP in both the time and frequency domains. They also found that the amplitude of the peaks of movement evoked potentials (mEPs) and cue evoked potentials (cEPs) varied with direction. A characteristic waveform that appears in an LFP signal time locked to an event is called an *evoked potential*. Evoked potentials are calculated by averaging LFP signals over trials time aligned to the event of interest (see [59]); this reveals any consistent modulation or activity. Rickert et al. reported two positive (P1, P2) and two negative (N1, N2) peaks in the mEP and cEP, and found that across all 419 LFP recordings over all sessions in the contralateral and ipsilateral hemispheres, 16% of the mEP's were tuned during P1, 38% during N1, 48% during P2 and 50% during N2. They also found that the three frequency bands (≤ 4 , 6 – 13 and 63 – 200 Hz) were directionally modulated [35]. The spectra of the individual LFP signals were very similar on average in all of the frequency bands. However, they did not report the percentage of LFP signals tuned in the frequency domain, or the distribution of preferred directions in either the frequency or time domains.

Heldman et al. also reported directional modulation in the 18 – 26, 30 – 80 and 60 – 200 Hz bands (10.5%, 12.5% and 14.9% of recorded M1 LFP's were significantly tuned), in a 3D reach task. Scherberger et al. showed that LFP's in the posterior parietal cortex modulated with the direction of reaches and saccades prior to execution [22]. Richardson also reported that power in both the beta and gamma bands varied with the direction of movement [60]. Tuning in the beta band was largely bimodal, while gamma tuning was largely unimodal. Preferred directions for beta oscillations were not uniformly distributed and clustered around certain values.

After this, O'Leary and Hatsopoulos [61] reported tuning in mEP's and cEP's of LFP's calculated separately for three frequency bands: < 10 , 10 – 25 and 25 – 45 Hz. Interestingly, they also reported that within a given cortical area and data set, the preferred directions for each of these three groups were clustered in few (and often just one) groups. Different data sets and recording sessions had their preferred directions clustered around different points.

This chapter explores the use of LFP from the contralateral and ipsilateral hemispheres as a direct BMI input to predict movement. The first section of this chapter delves into directional modulation in LFP signals from an implanted micro-electrode array, and par-

ticular issues that may arise from the strong correlations between the signals. The second section details and tests an algorithm for LFP based offline movement prediction.

4.1 Direction Modulation

We investigated the directional modulation of the power of the LFP signal in the 0 – 10 Hz, 15 – 45 Hz (beta) and 60 – 100 Hz (gamma) bands, as well as in the mEP and cEPs.

4.1.1 Modulation Methods

The animal behavior, data collection and data analysis were performed as described in Chapter 2. We considered directional modulation of power in the 0 – 10 Hz, 15 – 45 Hz (beta) and 60 – 100 Hz (gamma) bands during the hold period (HP), defined as 500 ms prior to movement onset, movement period (MP) and target hold period (THP). Trials were classified based on the direction of movement. In order to be able to compare modulation across days of recording, we subtracted the mean of all LFP signals from each LFP signal prior to evaluating the spectra. Using the LFP signal on one electrode, we calculated the average power in each band during HP, MP and THP for each direction.

We used an ANOVA ($p < 0.05$) to test the significance of any modulation observed. Similar to tuning curves for spike data, we normalized the tuning curves and fit these to a cosine curve as in [58], to calculate the preferred direction.

To calculate the mEPs and cEPs we averaged the raw LFP signal aligned with the go cue and movement onset [59]. While the timestamp for the go cue was recorded by the Plexon software, movement onset was calculated using the hand’s velocity profile. For this chapter, the movement onset was recorded when the velocity crossed a predetermined threshold (1 cm/sec). To calculate separate evoked potentials for each direction, we classified trials based on the direction of movement and then averaged the LFP signals. We used the peak-to-valley depth, peak height, valley height or area under the peak of the evoked potential as metrics to calculate tuning.

4.1.2 Modulation Results

Tuning in Frequency Domain

Results in this section use data under the MC paradigm. The data from monkey P showed significant modulation of power in the beta band during the hold period, consistent with the results of [61]. Figure 4.1 shows averaged spectrograms for each movement direction. Beta power during the hold period (500 ms prior to movement onset at 1000 ms) varies with direction, and is maximized during reaches to 225° and 270° . The 0 – 10 Hz band is high during THP, but was not significantly tuned to one direction. Spectrograms did not show significant modulation in the gamma band. The results in the gamma band conflicts with the results of Rickert and Heldman, and are further explored in the discussion section.

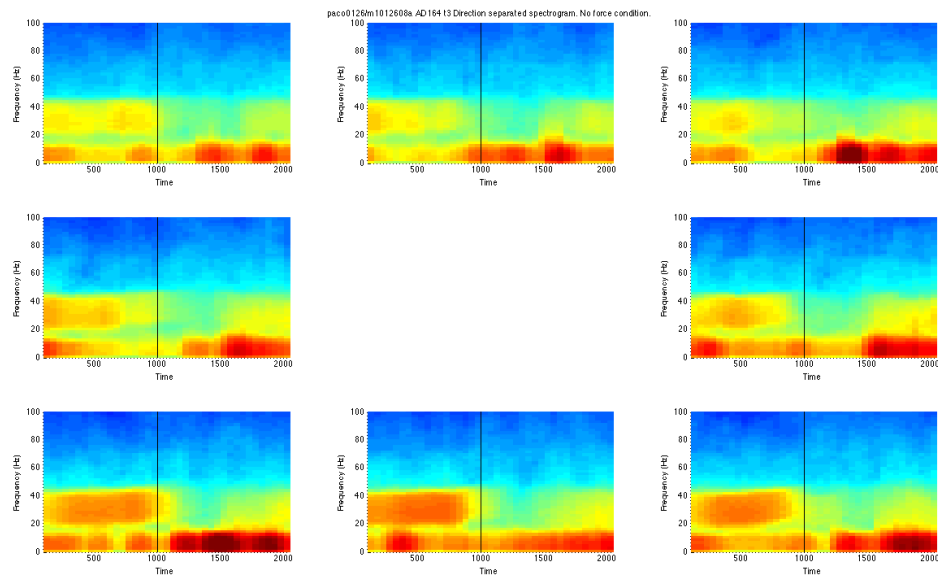


Figure 4.1. Session-average spectrograms for each movement direction. Beta power during the hold period varies with direction, but there are no apparent changes in the gamma band. The directions represented are: anti-clockwise from middle-right: 0° – 315° in increments of 45° .

Power on each electrode varied almost identically with direction - most signals had maximum power in the beta band for reaches to 225° and 270° , and thus preferred directions in this range. This modulation also remained constant across days. This raises questions regarding the validity of the tuning observed. Is this a reflection of the high correlation of

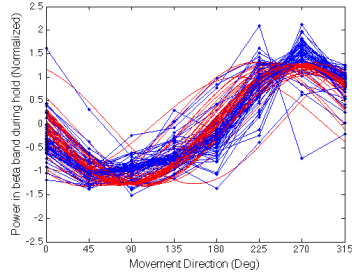
the LFP signals? If so, does the difference in preferred direction change as distance between electrodes increases? This remains to be investigated.

Does this constant modulation arise from a common noise signal or noise reflected in the common reference for each electrode? To test this, we considered the mean of all LFP signals over electrodes, which would reveal any common noise signal in the reference. We subtracted the mean of LFP signals across electrodes from each signal before calculating tuning curves to eliminate this possibility. Preferred directions for signals remained the same both with and without the common mean subtracted.

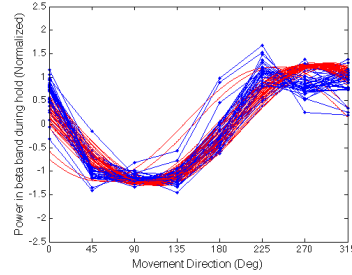
Figure 4.2 shows the tuning curves and the cosine fit for each curve for all 64 electrodes in M1 (with mean subtracted) on six days: Day 1 and Day 30 – 34. The tuning curves of some electrodes on which signals were known to be noisy are not shown. Note the outlier on Day 15 whose preferred direction does not cluster with the other signals. We could not identify this electrode as noisy and could not explain why it does not cluster with the other electrodes. We accounted for the larger standard deviation this leads to while analyzing the clustering of the signals in table 4.1.

A large percentage of the 64 electrodes showed significant (ANOVA) direction tuning. Table 4.1 shows the percentage of the 64 signals that were tuned each day, as well as the distribution of preferred directions across electrodes and recording sessions. The last column shows that large percentage of the tuned signals each day cluster around a mean preferred direction. This suggests that the preferred directions of LFP beta tuning also cluster in a group, similar to the observations by O’Leary and Hatsopoulos [61]. However, they also report a change in clustering over days, which we do not observe in our data. Also, while we compute the average power in a band, [61] looks at evoked potentials arising in the frequency band.

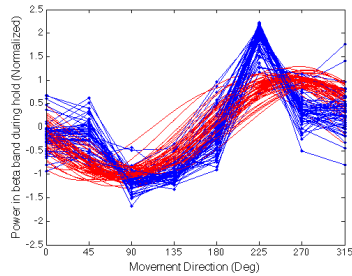
Preliminary analysis in monkey R also showed similar clustering of LFP beta tuning. We do not believe that the clustering in our LFP data is due to a common noise source, but it is difficult to conclusively eliminate this possibility without extensive further experiments. This could be the basis for a set of future experimental research. In addition, we observed that the tuning in the ipsilateral cortex was very similar to that in the contralateral cortex. The precise direction tuning in the ipsilateral cortex also remains to be further investigated.



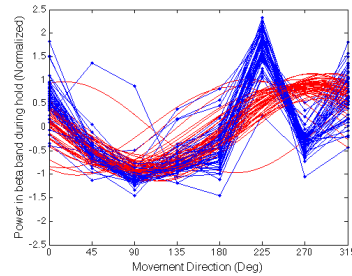
(a) Day 1



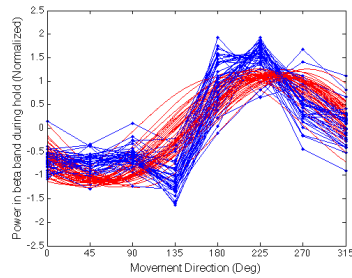
(b) Day 13



(c) Day 14



(d) Day 15



(e) Day 16

Figure 4.2. Tuning curves for beta power in M1 in the LFP during hold period. Tuning curves remain similar over a period of thirty days, as well as over five continuous days. Each subfigure plots the normalized beta power v/s the direction of movement (blue curves) for all 64 electrodes in the M1 array. The red curves are the best sinusoidal fit to each curve. Thus tuning remains constant over days and over electrodes.

Table 4.1. Distribution of LFP preferred directions across electrodes and days

Day	% significnatly tuned	Mean PD (deg)	PD Std Dev (deg)	% tuned within 1 std of mean
Day1	86	266.81	19.37	83
Day 13	58	280.4	13.40	81
Day 14	87	261.50	17.60	75
Day 15	76	269.98	43.66	91
Day 16	64	234.73	(outlier fig 4.2(d)) 18.58	within $\pm 15 = 86$ 68

Tuning in Evoked Potentials

We observed cue and movement evoked potentials (cEP and mEP), similar to those in [35]. Since the precise time of movement onset was hard to determine (see 4.1) the cEP was much cleaned than the mEP. Nevertheless, some directional modulation was visible in the shape of the cEP and the mEP (figures 4.3 and 4.4). Using the peak-to-valley depth, peak height, valley height or area under the peak as metrics we were unable to find significant unimodal tuning in the cEP or mEP. Decomposition of the evoked potential into different frequency bands as in [61] may lead to unimodal tuning; and could be investigated as future work.

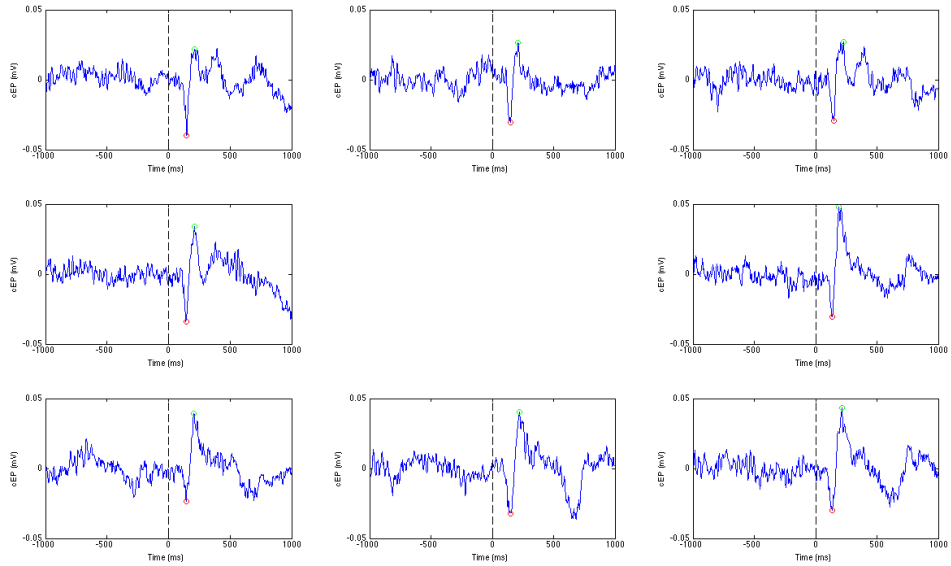


Figure 4.3. Cue evoked potentials for reaches to targets in each of eight directions. The red circle represents the peak of the evoked potential and the green circle the valley. The directions represented are: anti-clockwise from middle-right: $0^\circ - 315^\circ$ in increments of 45° .

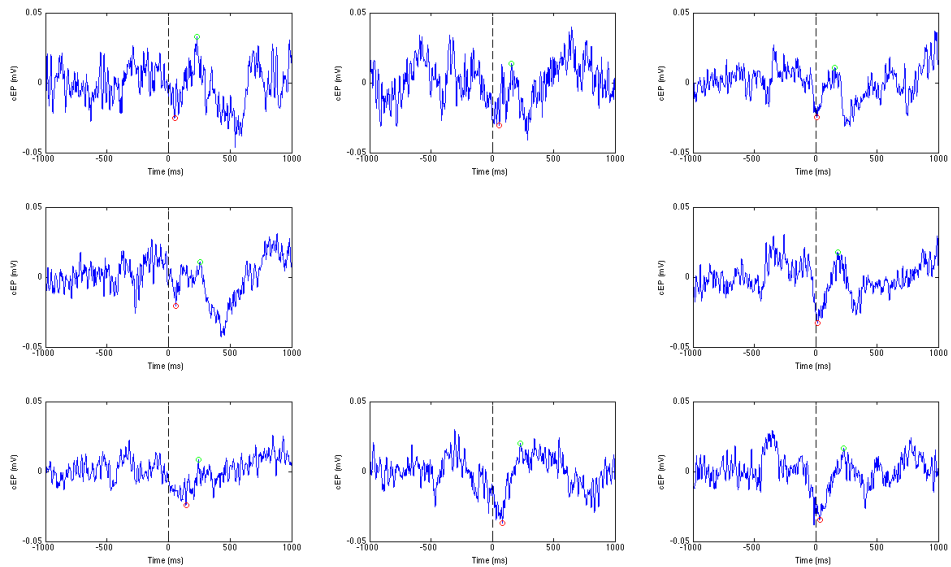


Figure 4.4. Movement evoked potentials for reaches to targets in each of eight directions. The red circle represents the peak of the evoked potential and the green circle the valley. The directions represented are: anti-clockwise from middle-right: $0^\circ - 315^\circ$ in increments of 45° .

4.2 Offline Movement Prediction

Using the spectral decomposition of the LFP signal, and a simple lagged linear model, we predicted cursor position under MC, using signals from M1 and ipsilateral M1 separately. Thus, there was no feedback (visual or otherwise) signal provided to allow any adaptation by the linear model.

4.2.1 Prediction Methods

We recorded the position of the cursor (and hand) in joint coordinates (shoulder and elbow angle) using the KINARM. A linear model (wiener filter), similar to the filter used in [10] was trained and used to predict movement.

The offline prediction algorithm used the spectral decomposition of the LFP signal as input to a Wiener filter to predict movement. For this we calculated the power of the LFP in 10 Hz blocks i.e., 1 – 10 Hz to 90 – 100 Hz, using the multi-taper spectral estimation technique, as described in the Methods section. We calculated a power estimate every 50 ms, using a window of ± 100 ms, and $K = 5$.

We generated time series of powers in the five bands (sampled at 20 Hz, i.e. one point every 50 ms). We also allowed the use of 500 ms of history (10 lags). For completeness, we included the raw LFP time series as an input; however, it must be noted that results without the time domain information were slightly better than those including time domain information. This may be due to the additional noise introduced by the time series. Thus, one LFP signal led to $50 + 1 = 51$ input signals to a Wiener filter. We used information from 6 electrodes chosen uniformly from the array, since results using fewer and more than six electrodes were worse. The filter was trained on 8 – 12 minutes of data (depending on the session) and was used to predict the last 2000 ms of movement over 4 days.

4.2.2 Prediction Results

Figures 4.5 and 4.6 plot the actual and predicted movement from one session in joint co-ordinates for the predictions using M1 and ipsilateral M1 respectively. The correlation coefficients of the predicted and actual movement traces in these figures are given in table 4.2. These coefficients are lower than those typically observed for spike data, and we can see the prediction noise in figures 4.5 and 4.6. The prediction scheme showed consistent

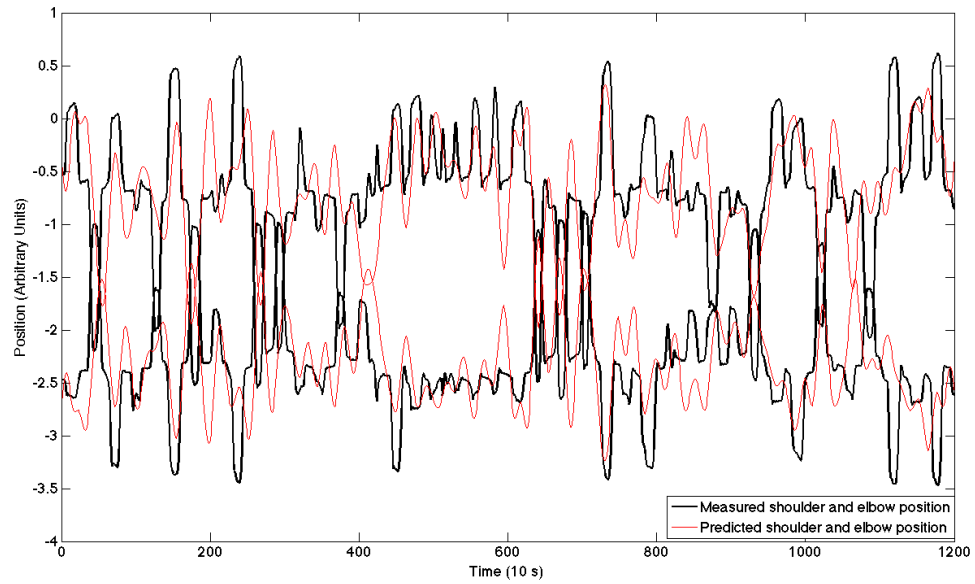


Figure 4.5. Movement prediction using spectral decomposition of contralateral M1 LFP.

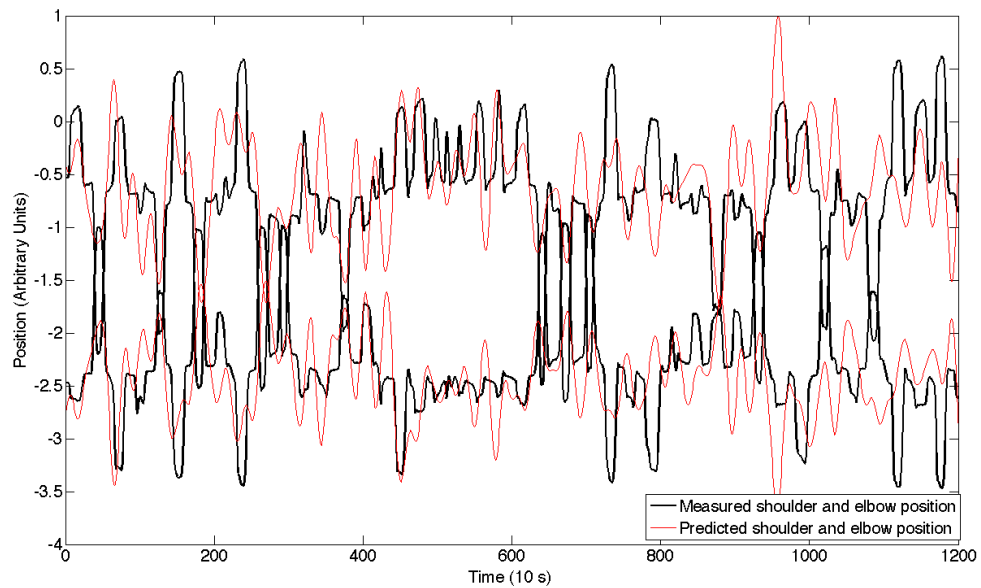


Figure 4.6. Movement prediction using spectral decomposition of ipsilateral M1 LFP.

results over days for both Monkey P and Monkey R. Tables 4.3 and 4.4 shows the average correlation coefficient obtained over days for Monkey P and Monkey R respectively.

Table 4.2. Correlation coefficients between predicted and actual movement

	Shoulder	Elbow
M1	0.59	0.61
M1 Ipsi	0.49	0.50

Table 4.3. PACO: Correlations coefficients for predictions of Shoulder and Elbow angles and X & Y positions and velocities using LFP electrodes in the contralateral and ipsilateral hemispheres respectively, using 6 LFP signals in the time and frequency domain.

Variable		Day 1	Day 2	Day 3	Day 4	Day 5	Mean	Std Dev
Shoulder	Contra	0.6462	0.5275	0.6236	0.6641	0.4966	0.5916	0.0748
	Ipsi	0.4716	0.3542	0.4343	0.4824	0.4442	0.4374	0.0504
Elbow	Contra	0.6068	0.6195	0.6425	0.6376	0.5230	0.6059	0.0485
	Ipsi	0.4744	0.4303	0.4840	0.5052	0.5102	0.4808	0.0318
X position	Contra	0.5861	0.4365	0.3188	0.4629	0.4859	0.4581	0.0962
	Ipsi	0.2520	0.4786	0.1811	0.4378	0.0808	0.2861	0.1691
Y position	Contra	0.6011	0.5863	0.6437	0.6059	0.5095	0.5893	0.0494
	Ipsi	0.4461	0.3828	0.5027	0.4748	0.4812	0.4575	0.0464
X velocity	Contra	0.0555	0.0246	0.0156	0.0568	-0.0534	0.0198	0.0449
	Ipsi	0.1523	0.0521	-0.1297	0.1970	-0.0414	0.0461	0.1347
Y velocity	Contra	-0.0713	0.0918	-0.0623	0.1848	0.0103	0.0307	0.1083
	Ipsi	0.2081	0.2074	0.1118	0.0166	0.0899	0.1268	0.0819

Table 4.4. RICO: Correlations coefficients for predictions of Shoulder and Elbow angles and X & Y positions and velocities using LFP electrodes in the contralateral and ipsilateral hemispheres respectively, using 6 LFP signals in the time and frequency domain.

Variable		Day 1	Day 2	Day 3	Mean	Std Dev
Shoulder	Contra	-	-	0.4170	0.4170	-
	Ipsi	0.3188	0.4272	0.3724	0.3728	0.0542
Elbow	Contra	-	-	0.4140	0.4140	-
	Ipsi	0.4470	0.5286	0.3908	0.4555	0.0693
X position	Contra	-	-	0.3633	0.3633	-
	Ipsi	0.2410	0.4075	0.2471	0.2985	0.0944
Y position	Contra	-	-	0.4050	0.4050	-
	Ipsi	0.4280	0.5236	0.3965	0.4494	0.0662
X velocity	Contra	-	-	0.2504	0.2504	-
	Ipsi	0.0375	0.0895	-0.0038	0.0411	0.0467
Y velocity	Contra	-	-	-0.0444	-0.0444	-
	Ipsi	0.0432	-0.1224	-0.2612	-0.1134	0.1524

4.3 Discussion

The recorded LFP signal shows directional modulation, supporting the results of [35]. The results did not show tuning in the gamma band. This conflicts with the results of Rickert and Heldman. However, Rickert did not report numbers on how many LFPs were tuned, and only 14.9% of the signals from the Heldman paper were significantly tuned in the gamma band. Based on purely ANOVA significance testing, some of the LFPs were tuned in the gamma band i.e. there was significant difference in the gamma powers for different directions. However, very few of the signals were thus tuned, and they did not show clean tuning curves, and hence we dismissed these as chance.

The preferred direction was fairly constant across multiple electrodes and recording days. Single unit activity recorded from the same electrodes did not show any clustering of preferred directions (unpublished observations). This similarity of preferred directions is not surprising given the high correlations between LFP signals, in the time and frequency domains, as suggested in chapter 3. [61] and [60] have recorded similar clustering of LFP preferred directions. [61] suggests that this correlation may be due to the volume conduction of synchronous post-synaptic potentials from neighboring neural populations. Another hypothesis to explain preferred direction clustering might be that the direction tuning in LFP represents a bias in the direction tuning of single units. We did not find any relationship

between the average population vector over a session of the single unit activity and the preferred direction of the LFP.

Does the similarity of preferred directions across LFP signals simply reflect that limb movements are anisometric, instead of revealing LFP information content? The anisometric nature of movements has been previously noted in this context [58], [60]. Given the similarity of preferred directions across electrodes, we cannot calculate an analogue of the population vector for LFP signals, i.e. different electrodes cannot be used (as different cells might be) to encode for movements in different directions. Can we still use LFP a BMI control on a single trial basis? We may still be able to harness the observed modulation to predict the direction of movement in a BMI. The amplitude of beta oscillations could be used as an 8-bit classifier to indicate the direction of movement. Also, our results in directional modulation are limited to the MC mode. It would be interesting to see if similar patterns in the preferred direction are found during BC mode as further work.

The work in this thesis is a first attempt at using the spectral decomposition of LFP for direct BMI prediction. Both the ipsilateral and contralateral LFP signal can be used for open loop or offline movement prediction with consistent and high correlation coefficients. An interesting observation is the similarity of the directional modulation of the ipsilateral and contralateral cortices, which is again not surprising given the highly correlated LFP in both hemispheres, but suggests that LFP in both cortices may carry similar information. Related work (to be published) [62] further discusses the importance of the ipsilateral cortex towards BMI development.

It is important to note that LFP predictions perform significantly worse than predictions from spike data from previous studies, for instance the offline predictions of [63]. However the LFP performs better than EEG or ECoG control [14]–[18]. We have not conducted any experiments to test online LFP control with visual feedback. Such an experiment would help further understand the utility of the LFP.

Chapter 5

Beta band oscillations

Oscillatory behavior in neural recordings have been related to higher order sensory processing, inter- and intra-cortical communication, facilitation of synaptic plasticity and long-term information consolidation [23], [47]. Beta and/or gamma synchronization could mediate interactions and subserve long range functional coupling [51], [64]. Beta waves propagate across the motor cortex as a traveling wave, supporting the hypothesis that these oscillations are relevant to intra- and inter-cortical information transfer [27]. Oscillations in the gamma band have been associated with attention during visual tasks such as change detection and shape tracking [29], [65]. In this chapter, we investigate local field potential (LFP) beta oscillations as control inputs for brain-machine interfaces (BMIs).

BMIs are devices that decode neural activity to control external devices such as computer cursors or mechanical actuators. LFPs have been previously used in BMIs to control a virtual finger and to predict movement trajectories through the control of a computer cursor [19], [20]. We focus on LFP oscillations in the beta band (15-45 Hz [27]), which may be particularly relevant to develop BMIs. Beta oscillations have been thought of as indicative of movement preparation [36], attention to fine control [53], a correlate of ‘idling’ motor neurons [66], or an indication that the motor cortex is performing a task of low complexity (such as maintaining a posture) [37].

Previous works have reported LFP oscillations in the beta range prior to movement initiation and during steady posture or grip hold for a motor task [27], [36], [37]. A drop in beta power accompanies movement onset. Beta oscillations in human EEG recordings during motor tasks note similar results [66]. However, Murthy and Fetz observed more

prominent beta oscillations during unconstrained motor tasks and exploratory tasks in an occluded area than during rest or over-trained movements [28], [53]. It has been observed that beta power in EEG increases with practice across days in a task to control a hand orthosis using EEG signals [67].

In this chapter, we investigate beta oscillations in the LFP signal recorded during a motor task under two conditions: (1) the subject uses its arm to complete the task and (2) the subject, without overt limb movement, completes the task by generating a control signal based on its neural firing rates, similar to standard BMI paradigms used previously [10]. Ranade et al. discusses a chunk of the results presented here [68].

5.1 Methods

Experimental design, behavior and data collection methods are the same as described in chapter 2. Figures in this chapter are referenced to the movement onset and presented on a logarithmic scale with arbitrary but uniform power units across figures. However, we observed similar results with respect to go cue. The beta power profile (15 – 45 Hz) over a trial gives the average power over the beta frequencies every 50 ms. The beta profile over one trial was calculated as the average power over the beta frequencies (20-45 Hz) in a given time window.

In this chapter, movement onset was recorded as the cursor left the center target. We defined the hold period (HP) as the 500 ms immediately prior to movement onset and the initial movement period (IMP) as the first 500 ms after movement onset.

5.1.1 Spike Triggered Averages

To calculate spike triggered averages (STAs) we averaged the LFP signal in a ± 125 ms window around each spike on an electrode, aligned to the spike time over the whole session. Fourier transforms of the STAs provide spike-field coherence [29] to clarify phase locking to any frequency.

5.1.2 Prediction algorithm

We used the power in the beta band across all electrodes in M1 to predict stationarity of the BMI cursor in BC mode. Time along a trial was divided into 50 ms windows. If the power in the beta band on an electrode in a window was greater than the average beta power over the session, the algorithm predicted stationarity of the cursor for the following 200 ms.

5.2 Results

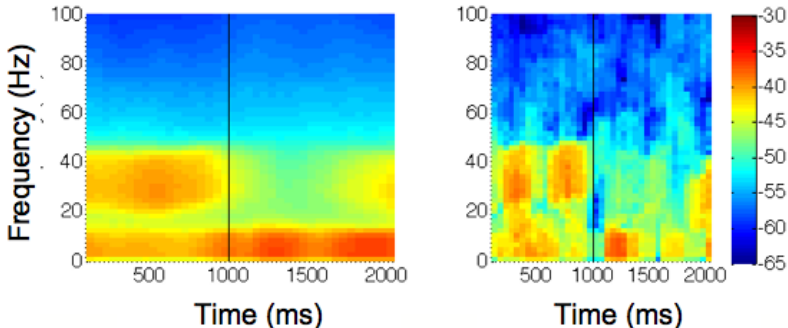


Figure 5.1. Manual Control: Average (left) and single trial (right) estimate of the PSD of the LFP signal on one electrode on a logarithmic scale (arbitrary units). Movement onset is at 1000ms. For most trials beta power increases during the hold period and drops after movement onset.

Each recording session lasted about 2 hours per day, during which the subject performed 200 – 300 trials in MC and BC modes. The subjects were over-trained in the MC task; a reach was 0.7 s. Reaches in the BC mode took longer on average (2 s) and followed a stop-go structure as the animal attempted to reach the target. No overt arm movements were observed in BC mode.

Figure 5.1 shows the trial average spectrogram estimates of the LFP over one session-aligned to movement onset, as well as a representative single trial spectrogram in MC. As noted in [27], [36], [37], there is sharp drop in beta power with movement onset in manual control, which lasts the duration of the movement. Also, we often see an increase in the beta power during the target hold period, indicated by the increase in beta power around 2000 ms in the average MC plot.

Notably, there is also a sharp drop in beta power immediately after movement onset

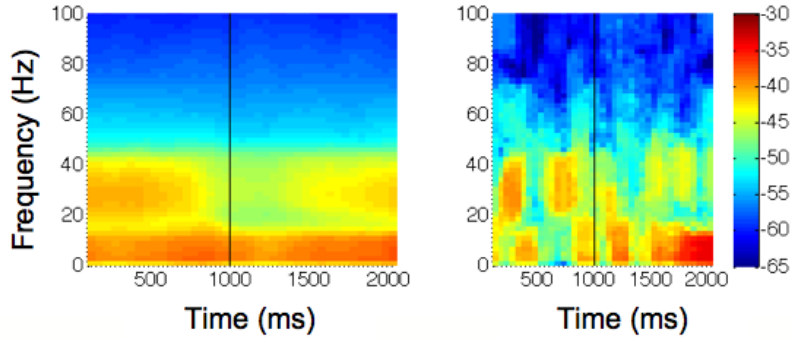


Figure 5.2. Brain Control: Average (left) and single trial (right) estimate of the PSD of the LFP signal on one electrode on a logarithmic scale (arbitrary units). Movement onset is at 1000ms. Similar to manual control, beta power increases during the hold period and drops after movement onset.

in BC mode, which lasts for about 500 ms on average as seen in figure 5.2. The longer reaches in BC mode and the stop-go nature of the reach lead to intermittent bursts of beta power during individual trials. The change in beta power between the HP and the IMP was significant at the 5% level across all five days examined under both MC and BC.

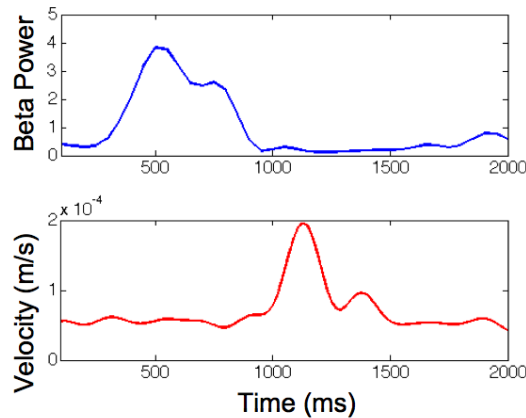


Figure 5.3. Beta power and velocity in MC. The cursor leaves the center target at 1000 ms.

We observe high beta power in MC (compared to the average power) only when cursor velocity is close to zero. For each trial, beta power drops as the cursor leaves the center target and velocity increases (at 1000 ms in figure 5.3). Beta power remains low throughout the movement. We see from figure 5.4 that high beta power and high velocity do not occur simultaneously across all trials in a session. Using a set threshold (10^{-4} units, see section 5.1) we classified points along the trial as high (blue) and low beta (green) power. The mean velocity of the hand during high beta periods in a session was significantly smaller

than the velocity during low beta power ($p = 0.05$). This significant difference was observed even if we used the average beta power across the session as a threshold.

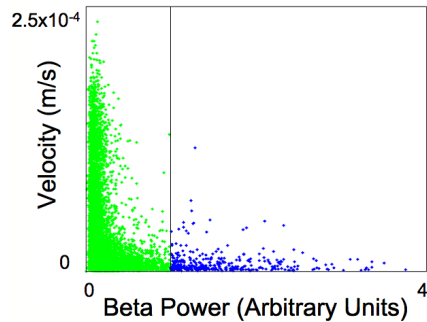


Figure 5.4. Hand velocity v/s beta power in MC. The points do not span the space and high beta power and high velocity do not occur simultaneously.

Although the movements in BC mode have greater variance in their position and velocity profiles, high velocity cursor movements rarely occur during periods of strong beta oscillations. Velocity is zero at the same time as the beta power peak in figure 5.5, while the beta power is low during high velocity cursor movement. There was a significant difference ($p = 0.05$) between the mean velocities over the high and low beta conditions in BC mode as well (threshold 10^{-4} units), as illustrated in figure 5.6. Similar results were observed for a second subject.

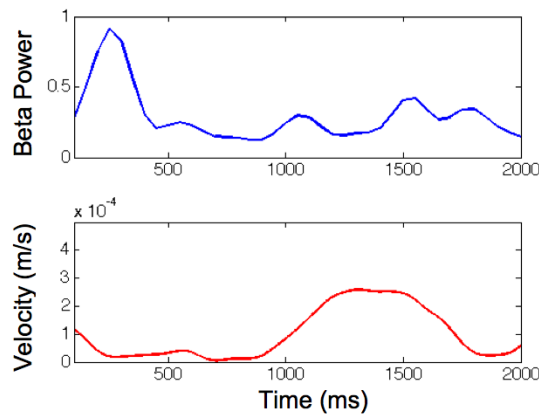


Figure 5.5. Beta power and velocity in BC. The cursor leaves the center target at 1000 ms.

We observed that cursor velocity in both MC and BC modes was low for about 200 ms following peaks in the beta power and used this to design a simple offline algorithm to predict cursor stationarity for 50 ms windows (described in Methods). Thus for each HP

(and IMP) the algorithm predicts that the cursor is stationary for a certain percentage of time.

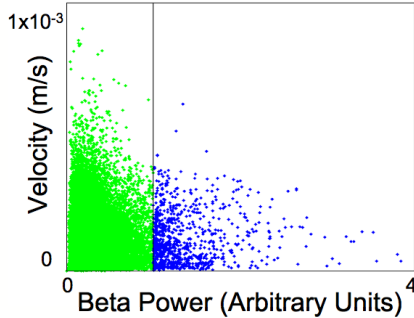


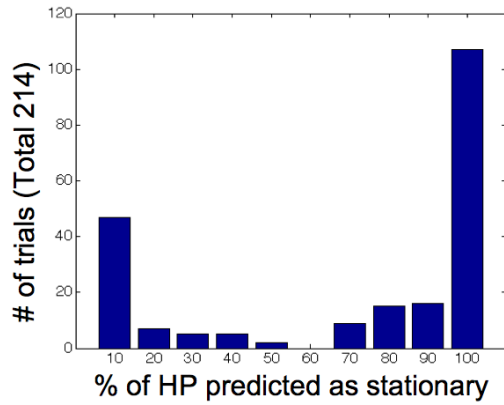
Figure 5.6. Hand velocity v/s beta power in BC. As in figure 5.4, high velocity and high beta power do not occur simultaneously.

For each trial, we calculated the percentage of time that the algorithm predicted stationarity during the HP (and IMP). A prediction of stationarity during the HP was considered a correct prediction, since the subject is expected to be stationary at this time, whereas a prediction of stationarity during the IMP was considered a false alarm. For approximately 150 (of 214) trials, $> 70\%$ of the HP was predicted as stationary (figure 5.7(a)). We observed significant false alarms for 60 (of 214) trials were false alarms, where $> 70\%$ of the IMP was also predicted to be stationary (figure 5.7(b)), however for the majority of the trials $< 10\%$ of the IMP was predicted as stationary.

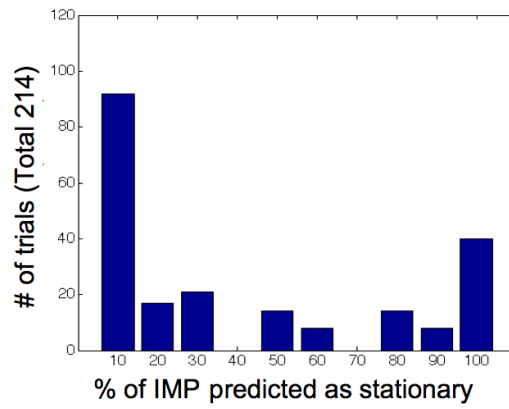
5.2.1 Spike triggered averages

Spikes recorded on an electrode phase locked to the LFP beta oscillations recorded on the same or different electrodes, consistent with previous observations by Murthy and Fetz, and Baker et. al [28], [37]. We see prominent oscillations in the time domain and a peak around 30 Hz in the spectra of the STA's over the hold period of manual control (figure 5.8(a)). Spikes did not phase lock to any frequency during the movement period.

We also found spikes that phase locked to the beta oscillation during periods of high beta in the BC mode. Figure 5.8(b) shows the STA for a neuron that was not involved as one of the neurons controlling the BC cursor. Though the signal in time domain is not as clean as in MC, we can see an underlying beta oscillation. The Fourier transform of the STA shows a peak at 30 Hz as well as a lower frequency to which the spikes are phase locked. If we assume that spikes are responsible for generating the LFP signal, the similarity of phase locking in BC and MC could suggest that the underlying processes generating the

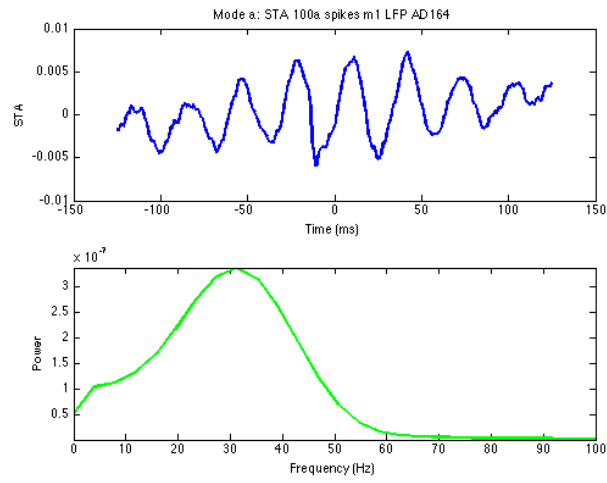


(a) Hold Period

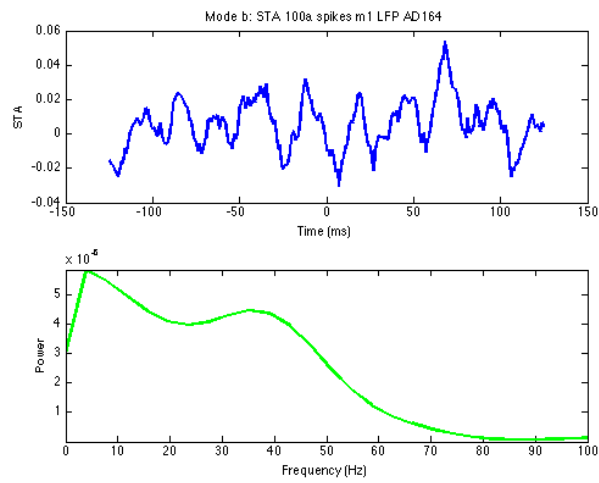


(b) Initial Movement Period

Figure 5.7. Algorithm analysis: (a) Histogram of stationarity predictions during the hold period over all trials. (b) Histogram of stationarity predictions during the movement period over all trials.



(a) Manual



(b) BMI

Figure 5.8. Spikes phase lock to beta oscillations in MC and BC. (Electrode not involved in BMI)

beta oscillation are similar in both modes. If we assumed the opposite however, that the LFP was in fact used as a timing device to synchronize spiking activity, we might be able to conclude that beta oscillations share functionality in both modes. However, much work needs to be done to further explore the generation of beta oscillations in LFP, before we can understand this further.

5.3 Discussion

It is known that beta power in the motor cortex is high during stationary task periods and decreases during movement periods for manual control [27], [36], [37]. We report that the beta power follows a similar pattern even during brain-control. With this information we can predict whether the BMI cursor should be stationary during a certain period. This result has implications for the development of future BMIs. High beta power, as an indicator of stationarity, could be used as a toggle switch for a BMI device.

The results presented in this paper also offer an insight into the nature of the beta rhythm. Baker et al. suggest that regular beta oscillations form a highly predictable signal of low entropy, and thus one which could not be used to convey much information [37]. They argue that the cortex can only afford such oscillations during a low complexity task, such as maintaining posture, as opposed to a more complex reach or grip task. This hypothesis and the observed pattern of beta oscillations would suggest that movement in BC is a more complex task than position maintenance. While the precise causal relationship between firing patterns and limb movement during MC is unknown, a precise model is used to control the cursor position under BC. In BC, holding a position requires maintenance of a precise firing pattern, while a specific movement requires the generation of a different pattern. Since the relative complexity of a change in firing rate compared to maintenance of a certain firing rate is unclear, we cannot easily explain the differences in BC beta power using Baker’s hypothesis.

Pfurtscheller et al. suggested that beta oscillations might be indicative of an idling state [66]. This seems unlikely given the constancy of firing patterns the subject must maintain during the hold and movement periods of BC. For instance, a specific firing pattern is required throughout the hold period; even a small change could result in cursor movement. Similarly, a specific firing pattern is required for movement in a specific direction. Sanes and Donoghue suggested that beta oscillations may be “related to aspects of movement preparation” [36]. However, it has been difficult to find relationships between beta power

in the motor cortex and task performance or attentiveness, as opposed to visual tasks where gamma oscillations correlate with these variables [29]. We did not find any obvious correlations between beta power and reaction time (time between the go cue and movement onset) or the time of reach, which agrees with the results presented in [36]. Instead of planning functions, beta oscillations may serve as a low energy state that the cortex reverts to in the absence of explicit movement.

In summary, we have shown that a basic algorithm can predict hold and movement periods in a trial. Such an algorithm could be used to supplement a firing rate based BMI to avoid unnecessary cursor noise during stationary periods, and thus improve the accuracy of a BMI that is primarily based on spike information.

Chapter 6

Conclusion

This thesis explores aspects of the LFP signal through the perspective of developing the next generation of BMIs. As the low frequency component of intra-cortical recordings, the LFP is noisier than, and not as effective as spike data when considered as a direct input to a BMI. Not surprisingly, movement predictions using the LFP as the only input to a BMI are far behind predictions using spike data. However, the results from this thesis indicate the utility of the LFP as a supplementary input to a spike controlled BMI. For instance, the direction tuning observed in the beta band of the LFP signal could be used as an independent validation mechanism for the movement predicted by spike data. We also found that the power in the beta oscillations of LFP is highly correlated with the movement state (stationary or moving) of a BMI cursor during both MC and BC. A reliable prediction of the stationarity of a BMI cursor could significantly reduce noisy movements during spike-based movement prediction.

The results of this thesis confirm previous work about LFPs and also indicate the significance of beta band of the LFP. We summarize them here:

1. Coherence calculations show that beta oscillations are pervasive in the cortex during the hold period during MC.
2. The power in the beta band of the LFP is significantly modulated by direction during MC. We find unimodal direction tuning (single peak in tuning curve) in the beta band, as compared to bimodal tuning (two peaks in tuning curve) previously observed [60]. Preferred directions of the signals on different electrodes cluster together, similar to the results of [60], [61].

3. Previous studies had noted higher power in the beta band during the hold period and lower power during the movement period in MC. The work in this thesis replicates previous results. Additionally we observe that the change in beta power movement during a BC task follow a pattern similar to MC. Even in BC, there is an increase in beta power during the hold period followed by a decrease on movement onset.
4. Beta oscillations can be used to predict the stationarity of the task cursor in both MC and BC.
5. Spikes phase-lock to beta oscillations during BC. Phase-locking during MC has been widely observed previously [28], [37]. This could suggest a similar function and/or origin for beta oscillations in BC and MC.

These results lead to many further questions and future projects to be pursued. Some of them are discussed below.

1. This thesis makes some observations about LFP-LFP coherence in the context of behavior. However, we still have no understanding of what coherence represents biologically. What are the implications of cortex wide beta coherence during the hold period? What does it mean to have coherence at only select frequencies?
2. Finite window sizes introduce artifacts in coherence calculations, and these parameters should be taken into consideration while comparing results across datasets and papers.
3. Similar to the results of Oleary and Hatsopoulos [61] and Richardson [60], we observed that LFP preferred directions in the beta range cluster close together. Unlike spikes, LFP signals may not be able to represent independent movement directions. Is the LFP preferred direction well defined if this direction is the same throughout the motor cortex? Is the constant direction tuning of the LFP signal purely a reflection of the anisometric nature of limb movements [58], [60]?
4. A natural next step from this thesis might be to conduct closed-loop feedback experiments using the LFP signal as a direct BMI controller. We hypothesize that this would work better than the open loop results predicted, but not as good as results using spike data. It has been observed that spike activity can be volitionally modulated [4], but volitional modulation of an LFP signal has yet to be observed. An LFP-based BMI experiment may help shed light on whether the LFP signal can also be volitionally modulated.

5. We still lack a clear understanding of the functionality of beta oscillations. Results from this thesis and other papers suggest that beta oscillations may serve as:
 - (a) idle oscillations, a default state that the cortex reverts to when no other important events are happening
 - (b) a carrier wave for communication
 - (c) a timing signal for spike synchronization across brain regions
 - (d) a ‘planning’ oscillation

However, we have no conclusive evidence to favor any hypothesis over the others.

Based on the work in this thesis and elsewhere, we know that the LFP is an information rich signal. However, we are fundamentally limited in our perspective during neural signal analysis since we can only analyze signals we can record - EEG, ECoG, LFP or action potentials. Our little understanding of brain functionality provides a limited understanding of what the LFP represents biologically, and our observations may be a byproduct of other underlying processes we are unaware of. There is much work to be done to gain a good understanding of the functionality of the LFP.

Our results show that the LFP can provide valuable supplementary information for a spike-based BMI. The direct use of LFP, as well as spike data, for BMI work is closely related to the development of recording technologies. There are many advances to be made in this field to achieve the goal of long-term stable recordings from electrodes that are implanted in humans. In the meanwhile, BMI experiments may continue to help us understand concepts like volition and plasticity, give us insight into the nature of brain signals and finally understand how the brain works.

References

- [1] A. Nobunaga, B. Go, and R. Karunas, "Recent demographic and injury trends in people served by the model spinal cord injury care systems," *Archives of Physical Medicine and Rehabilitation*, vol. 80, no. 11, pp. 1372–1382, 1999.
- [2] E. Schmidt, "Single neuron recording from motor cortex as a possible source of signals for control of external devices," *Annals of Biomedical Engineering*, vol. 8, no. 4, pp. 339–349, 1980.
- [3] E. Fetz and M. Baker, "Operantly conditioned patterns on precentral unit activity and correlated responses in adjacent cells and contralateral muscles," *Journal of Neurophysiology*, vol. 36, no. 2, pp. 179–204, 1973.
- [4] E. Fetz, "Volitional control of neural activity: implications for brain-computer interfaces," *The Journal of Physiology*, vol. 579, no. 3, pp. 571–579, 2007.
- [5] J. Chapin, K. Moxon, R. Markowitz, and M. Nicolelis, "Real-time control of a robot arm using simultaneously recorded neurons in the motor cortex," *Nature Neuroscience*, vol. 2, pp. 664–670, 1999.
- [6] A. Schwartz, X. Cui, D. Weber, and D. Moran, "Brain-Controlled Interfaces: Movement Restoration with Neural Prosthetics," *Neuron*, vol. 52, no. 1, pp. 205–220, 2006.
- [7] D. Heldman, W. Wang, S. Chan, and D. Moran, "Local field potential spectral tuning in motor cortex during reaching," *Neural Systems and Rehabilitation Engineering, IEEE Transactions on [see also IEEE Trans. on Rehabilitation Engineering]*, vol. 14, no. 2, pp. 180–183, 2006.
- [8] M. Serruya, N. Hatsopoulos, L. Paninski, M. Fellows, and J. Donoghue, "Instant neural control of a movement signal," *Nature(London)*, vol. 416, no. 6877, pp. 141–142, 2002.
- [9] D. Taylor, S. Tillery, and A. Schwartz, "Direct Cortical Control of 3D Neuroprosthetic Devices," *Science*, vol. 296, no. 5574, pp. 1829–1832, 2002.
- [10] J. Carmena, M. Lebedev, R. Crist, J. O'Doherty, D. Santucci *et al.*, "Learning to Control a Brain–Machine Interface for Reaching and Grasping by Primates," *PLoS Biol*, vol. 1, no. 2, p. e42, 2003.
- [11] M. Velliste, S. Perel, M. Spalding, A. Whitford, and A. Schwartz, "Cortical control of a prosthetic arm for self-feeding," *Nature*, no. current, 2008.
- [12] L. Hochberg, M. Serruya, G. Friehs, J. Mukand, M. Saleh, A. Caplan, A. Branner, D. Chen, R. Penn, and J. Donoghue, "Neuronal ensemble control of prosthetic devices by a human with tetraplegia," *Nature*, vol. 442, pp. 164–171, 2006.
- [13] G. Santhanam, S. Ryu, B. Yu, A. Afshar, and K. Shenoy, "A high-performance brain-computer interface," *Nature (London)*, vol. 442, no. 7099, p. 195, 2006.
- [14] J. Wolpaw, D. McFarland, G. Neat, and C. Forneris, "An EEG-based brain-computer interface for cursor control." *Electroencephalogr Clin Neurophysiol*, vol. 78, no. 3, pp. 252–9, 1991.
- [15] F. Cincotti, D. Mattia, C. Babiloni, F. Carducci, S. Salinari, L. Bianchi, M. Marciani, and F. Babiloni, "The use of eeg modifications due to motor imagery for brain-computer interfaces," *IEEE trans. Neural Syst. Rehab. Eng.*, vol. 11, pp. 131–133, 2003.
- [16] J. Millan, F. Renkens, J. Mourino, and W. Gerstner, "Noninvasive brain-actuated control of a mobile robot by human EEG," *IEEE Transactions on Biomedical Engineering*, vol. 51, no. 6, pp. 1026–1033, 2004.
- [17] T. Pistohl, T. Ball, A. Schulze-Bonhage, A. Aertsen, and C. Mehring, "Prediction of arm movement trajectories from ECoG-recordings in humans," *Journal of Neuroscience Methods*, 2007.
- [18] G. Schalk, K. Miller, N. Anderson, J. Wilson, M. Smyth, J. Ojemann, D. Moran, J. Wolpaw, and E. Leuthardt, "Two-dimensional movement control using electrocorticographic signals in humans," *Journal of Neural Engineering*, vol. 5, no. 1, pp. 75–84, 2008.
- [19] P. Kennedy, M. Kirby, M. Moore, B. King, A. Mallory, N. Inc, and G. Atlanta, "Computer control using human intracortical local field potentials," *Neural Systems and Rehabilitation Engineering, IEEE Transactions on [see also IEEE Trans. on Rehabilitation Engineering]*, vol. 12, no. 3, pp. 339–344, 2004.
- [20] C. Mehring, J. Rickert, E. Vaadia, S. de Oliveira, A. Aertsen, and S. Rotter, "Inference of hand movements from local field potentials in monkey motor cortex," *Nature Neuroscience*, vol. 6, no. 12, pp. 1253–1254, 2003.
- [21] A. Belitski, A. Gretton, C. Magri, Y. Murayama, M. Montemurro, N. Logothetis, and S. Panzeri, "Low-Frequency Local Field Potentials and Spikes in Primary Visual Cortex Convey Independent Visual Information," *Journal of Neuroscience*, vol. 28, no. 22, p. 5696, 2008.

- [22] H. Scherberger, M. Jarvis, and R. Andersen, "Cortical Local Field Potential Encodes Movement Intentions in the Posterior Parietal Cortex," *Neuron*, vol. 46, no. 2, pp. 347–354, 2005.
- [23] G. Buzsaki and A. Draguhn, "Neuronal Oscillations in Cortical Networks," *Science*, vol. 304, no. 5679, pp. 1926–1929, 2004.
- [24] C. Gray and W. Singer, "Stimulus-Specific Neuronal Oscillations in Orientation Columns of Cat Visual Cortex," *Proceedings of the National Academy of Sciences*, vol. 86, no. 5, pp. 1698–1702, 1989.
- [25] U. Mitzdorf, "Properties of the Evoked Potential Generators: Current Source-Density Analysis of Visually Evoked Potentials in the Cat Cortex," *International Journal of Neuroscience*, vol. 33, no. 1, pp. 33–59, 1987.
- [26] R. Canolty, E. Edwards, S. Dalal, M. Soltani, S. Nagarajan, H. Kirsch, M. Berger, N. Barbaro, and R. Knight, "High Gamma Power Is Phase-Locked to Theta Oscillations in Human Neocortex," pp. 1626–1628, 2006.
- [27] D. Rubino, K. Robbins, and N. Hatsopoulos, "Propagating waves mediate information transfer in the motor cortex," *Nature Neuroscience*, vol. 9, pp. 1549–1557, 2006.
- [28] V. Murthy and E. Fetz, "Oscillatory activity in sensorimotor cortex of awake monkeys: synchronization of local field potentials and relation to behavior," *Journal of Neurophysiology*, vol. 76, no. 6, pp. 3949–3967, 1996.
- [29] T. Womelsdorf, P. Fries, P. Mitra, and R. Desimone, "Gamma-band synchronization in visual cortex predicts speed of change detection," *Nature*, vol. 439, no. 7077, pp. 733–736, 2005.
- [30] B. Pesaran, J. Pezaris, M. Sahani, P. Mitra, and R. Andersen, "Temporal structure in neuronal activity during working memory in macaque parietal cortex," *Nature neuroscience*, vol. 5, no. 8, pp. 805–811, 2002.
- [31] M. Nicolelis, L. Baccala, R. Lin, and J. Chapin, "Sensorimotor encoding by synchronous neural ensemble activity at multiple levels of the somatosensory system," *Science*, vol. 268, no. 5215, pp. 1353–1358, 1995.
- [32] P. Fries, "A mechanism for cognitive dynamics: neuronal communication through neuronal coherence," *Trends in Cognitive Sciences*, vol. 9, no. 10, pp. 474–480, 2005.
- [33] P. Fries, J. Reynolds, A. Rorie, and R. Desimone, "Modulation of Oscillatory Neuronal Synchronization by Selective Visual Attention," *Science*, vol. 291, no. 5508, p. 1560, 2001.
- [34] P. Fries, S. Neuenschwander, A. Engel, R. Goebel, and W. Singer, "Rapid feature selective neuronal synchronization through correlated latency shifting," *Nature Neuroscience*, vol. 4, pp. 194–200, 2001.
- [35] J. Rickert, S. Oliveira, E. Vaadia, A. Aertsen, S. Rotter, and C. Mehring, "Encoding of movement direction in different frequency ranges of motor cortical local field potentials," *J. Neurosci*, vol. 25, no. 39, pp. 8815–8824, 2005.
- [36] J. Sanes and J. Donoghue, "Oscillations in local field potentials of the primate motor cortex during voluntary movement." *Proceedings of the National Academy of Sciences of the United States of America*, vol. 90, no. 10, p. 4470, 1993.
- [37] S. Baker, J. Kilner, E. Pinches, and R. Lemon, "The role of synchrony and oscillations in the motor output," *Experimental Brain Research*, vol. 128, no. 1, pp. 109–117, 1999.
- [38] M. Volgushev, M. Chistiakova, and W. Singer, "Modification of discharge patterns of neocortical neurons by induced oscillations of the membrane potential," *Neuroscience*, vol. 83, no. 1, pp. 15–25, 1998.
- [39] T. Sejnowski and O. Paulsen, "Network Oscillations: Emerging Computational Principles," *Journal of Neuroscience*, vol. 26, no. 6, p. 1673, 2006.
- [40] M. Hayes, *Statistical Digital Signal Processing and Modeling*. John Wiley & Sons, Inc. New York, NY, USA, 1996.
- [41] M. Jarvis and P. Mitra, "Sampling Properties of the Spectrum and Coherency of Sequences of Action Potentials," *Neural Computation*, vol. 13, no. 4, pp. 717–749, 2001.
- [42] D. Thomson, "Spectrum estimation and harmonic analysis," *Proceedings of the IEEE*, vol. 70, no. 9, pp. 1055–1096, 1982.
- [43] D. Percival and A. Walden, *Spectral Analysis for Physical Applications: Multitaper and Conventional Univariate Techniques*. Cambridge University Press, 1993.
- [44] [Online]. Available: <http://chronux.org/>
- [45] P. Mitra and H. Bokil, *Observed Brain Dynamics*. New York: Oxford University Press, 2008.
- [46] H. Berger, "Über das Electroencephalogramm des Menschen [On the EEG in humans]," *Arch Psychiatr Nervenkr*, vol. 87, pp. 527–570, 1929.

- [47] E. Salinas and T. Sejnowski, "Correlated neuronal activity and the flow of neural information," *Nature Reviews Neuroscience*, vol. 2, no. 8, pp. 539–550, 2001.
- [48] T. Burchell, H. Faulkner, and M. Whittington, "Gamma frequency oscillations gate temporally coded afferent inputs in the rat hippocampal slice," *Neuroscience Letters*, vol. 255, no. 3, pp. 151–154, 1998.
- [49] C. Andrew and G. Pfurtscheller, "Event-related coherence as a tool for studying dynamic interaction of brain regions," *Electroencephalography and Clinical Neurophysiology*, vol. 98, no. 2, pp. 144–148, 1996.
- [50] T. Womelsdorf, J. Schoffelen, R. Oostenveld, W. Singer, R. Desimone, A. Engel, and P. Fries, "Modulation of Neuronal Interactions Through Neuronal Synchronization," *Science*, vol. 316, no. 5831, p. 1609, 2007.
- [51] T. Womelsdorf and P. Fries, "The role of neuronal synchronization in selective attention," *Current Opinion in Neurobiology*, vol. 17, no. 2, pp. 154–160, 2007.
- [52] J. Schoffelen, R. Oostenveld, and P. Fries, "Neuronal Coherence as a Mechanism of Effective Corticospinal Interaction," pp. 111–113, 2005.
- [53] V. Murthy and E. Fetz, "Coherent 25- to 35-Hz Oscillations in the Sensorimotor Cortex of Awake Behaving Monkeys," *Proceedings of the National Academy of Sciences*, vol. 89, no. 12, pp. 5670–5674, 1992.
- [54] P. Lakatos, G. Karmos, A. Mehta, I. Ulbert, and C. Schroeder, "Entrainment of Neuronal Oscillations as a Mechanism of Attentional Selection," *Science*, vol. 320, no. 5872, p. 110, 2008.
- [55] V. Murthy and E. Fetz, "Synchronization of neurons during local field potential oscillations in sensorimotor cortex of awake monkeys," *Journal of Neurophysiology*, vol. 76, no. 6, pp. 3968–3982, 1996.
- [56] G. Carter, "Coherence and time delay estimation," *Proceedings of the IEEE*, vol. 75, no. 2, pp. 236–255, 1987.
- [57] P. Huybers. [Online]. Available: <http://www.people.fas.harvard.edu/~phuybers/Mfiles/index.html>
- [58] A. Georgopoulos, J. Kalaska, R. Caminiti, and J. Massey, "On the relations between the direction of two-dimensional arm movements and cell discharge in primate motor cortex," *Journal of Neuroscience*, vol. 2, no. 11, pp. 1527–1537, 1982.
- [59] S. Cardoso de Oliveira, A. Gribova, O. Donchin, H. Bergman, and E. Vaadia, "Neural interactions between motor cortical hemispheres during bimanual and unimanual arm movements," *European Journal of Neuroscience*, vol. 14, no. 11, pp. 1881–1896, 2001.
- [60] R. A., "Role of the precentral cortex in adapting behavior to different mechanical environments," Ph.D. dissertation, MIT, 2007.
- [61] J. O'Leary and N. Hatsopoulos, "Early Visuomotor Representations Revealed From Evoked Local Field Potentials in Motor and Premotor Cortical Areas," *Journal of Neurophysiology*, vol. 96, no. 3, p. 1492, 2006.
- [62] K. Ganguly, L. Secundo, G. Ranade, A. Orsborn, D. Dragan, J. Wallis, R. Knight, and J. Carmena, "Cortical representation of ipsilateral arm movements in monkey and man," 2009.
- [63] S. Kim, J. Sanchez, Y. Rao, D. Erdoğmus, J. Carmena, M. Lebedev, M. Nicolelis, and J. Principe, "A comparison of optimal MIMO linear and nonlinear models for brain-machine interfaces," *Journal of Neural Engineering*, vol. 3, no. 2, pp. 145–161, 2006.
- [64] N. Kopell, G. Ermentrout, M. Whittington, and R. Traub, "Gamma rhythms and beta rhythms have different synchronization properties," pp. 1867–1872, 2000.
- [65] K. Taylor, S. Mandon, W. Freiwald, and A. Kreiter, "Coherent Oscillatory Activity in Monkey Area V4 Predicts Successful Allocation of Attention," *Cerebral Cortex*, vol. 15, no. 9, pp. 1424–1437, 2005.
- [66] G. Pfurtscheller, A. Stancák, and C. Neuper, "Post-movement beta synchronization. A correlate of an idling motor area?" *Electroencephalography and Clinical Neurophysiology*, vol. 98, no. 4, pp. 281–293, 1996.
- [67] G. Pfurtscheller, C. Guger, G. Müller, G. Krausz, and C. Neuper, "Brain oscillations control hand orthosis in a tetraplegic," *Neuroscience Letters*, vol. 292, no. 3, pp. 211–214, 2000.
- [68] G. Ranade, K. Ganguly, and J. Carmena, "LFP beta power predicts cursor stationarity in BMI Task," *Proceedings of the IEEE EMBS Conference on Neural Engineering*, 2009.